Deuterium transport and retention in the bulk of tungsten containing helium: the effect of helium concentration and microstructure

S. Markelj[a,*], T. Schwarz-Selinger[b] , M. Pečovnik[a], W. Chrominski[c], A. Šestan[a] and J. Zavašnik[a]

[a]*Jožef Stefan Institute, Jamova cesta 39, 1000 Ljubljana, Slovenia*
[b]*Max-Planck-Institut für Plasmaphysik, Boltzmannstrasse 2, D-85748 Garching, Germany*
[c]*Warsaw University of Technology Faculty of Materials Science and Engineering, Wołoska 141, Warsaw, Poland*

Abstract

The effect of helium (He) on deuterium (D) retention and transport in the bulk of tungsten (W) was investigated. For this purpose samples were irradiated by 500 keV He ions at 300 K to different fluences in order to obtain He maximum concentrations of 1 at.%, 3.4 at.%, and 6.8 at.% in 0.84 μm depth. In order to discern the effect of irradiation damage caused by He implantation from the effect of the pure He presence on D retention, the W samples were irradiated at 300 K by 20 MeV tungsten ions in advance to create displacement damage in the crystal lattice to a damage dose of 0.23 dpa. The samples were exposed to a D atom beam at 600 K with a flux of 3.5 $\times 10^{18}$ D/m^{2}s to populate all the created defects. The D depth profiles were measured in situ during and at the end of exposure by nuclear reaction analysis to follow the dynamics of the D uptake. Thermal desorption spectra were collected ex situ at the end of the exposure. We show that D retention increases with implanted He fluence linearly following a D/He ratio of 0.29. We obtained peaking of D concentration at the position of maximum He concentration, reaching for the 6.8 at.% He sample three times higher D concentration (1.1 at. %) than obtained on high dpa W ion irradiated samples (0.37 at. %) for the same loading conditions. D retention and transport was also studied on He containing samples that were annealed to 1700 K. There was no reduction of D retention in the He zone but 80 % reduction in the only W irradiated zone was observed, meaning displacement damage was almost completely removed. In the He zone the D concentration increased to 1.35 at.% and this we attribute to trapping of D around He bubbles of 1.5 nm size created at the He peak maximum as obtained by transmission electron microscopy. Neither in the as He implanted nor the 1700 K annealed sample He did act as diffusion barrier. From this study one can conclude that in the main wall of a future fusion device the effect of He will not dominate D retention in tungsten but at high heat flux areas where displacement damage possibly anneals out He could accumulate in the material that it could eventually dominate over the effect of displacement damage.

Keywords: Helium, Deuterium retention, NRA, TDS, He bubbles, Displacement damage, Tungsten

1. Introduction

In a future fusion device helium (He) will be produced directly through the deuterium-tritium fusion reaction, by nuclear reactions between the wall material and neutrons and indirectly by tritium decay. The 3.4 MeV α particles produced in the fusion reaction will transfer its energy to the plasma species and will arrive at the wall with relatively low energy (20-100 eV) [1]. With such low energy He will mainly affect the wall material near the surface by bubble growth and will alter deuterium (D) uptake and release at the surface [2, 3]. He produced through tritium decay or neutron-induced nuclear reactions will have an effect throughout the bulk of the material. From the calculation by Shimada et al. [4] one can expect to get about 600 atomic parts per million (appm) of He to be created due to tritium decay with the assumption that 1 at.% of tritium is retained in the wall. The contribution of He produced from the neutron-induced nuclear reactions depends very much on the choice of the wall material [5]. For tungsten (W) we can expect to get 30 appm after five full power years of neutron irradiation through neutron capture and alpha particle emission (n,α) in a fusion power plant [5]. One needs to stress that the emitted α particles have energies of the order of MeV, which means they will also cause displacement damage in the crystal lattice [5, 6]. It is worth mentioning that transmutation of carbon produces He under neutron irradiation as pointed out by Gilbert [5]. Therefore, carbon impurities in the tungsten material might increase the predicted He concentration in the material.

It was shown by theory that He is very mobile in tungsten [7] but is easily and strongly trapped by vacancies or other defects [8] and tends to cluster with other He atoms [9, 10]. Under certain conditions growth of He bubbles was observed, see e.g. [1] and references therein. This phenomenon itself is not yet fully understood, but is considered to be driven by He migration at high temperatures leading to bubble growth [1]. Formation of He bubbles may cause not only elastic but plastic deformation of the surface to form blisters that can eventually burst, causing surface erosion of plasma facing materials (PFMs) and plasma contamination. The presence of He in the material influences its macroscopic properties such as tensile strength, creep and fatigue behaviour or swelling [6]. Additionally, the possible high He inventory inside the bulk of PFMs can lead to He segregation at the grain boundaries (GB), forming a bubble network [1]. For example nano-bubble formation was observed by MeV He ion irradiation [11]. Such behaviour is even more probable at high temperatures, where for instance annealing of 1.3 MeV He-irradiated samples with a fluence of more than 10^{21} He/m^2 up to 2000°C lead to pronounced surface blistering

and exfoliation [11]. The reason is rapid He accumulation along GBs and dislocations, promoting inter-granular fracture known as helium embrittlement, which severely impairs the mechanical properties of PFMs.

He also influences the transport and retention of hydrogen isotopes (HI) close to the surface of the material. Recent experiments studying the interaction of HIs and He in tungsten using He seeded D plasmas showed that the addition of He leads to reduced blistering [12, 13]. Still, formation of nano-bubbles in the near surface layer was found [12], which was accompanied by a reduced D retention [2]. The formation of these nano-bubbles by few eV to keV He ion irradiation is fluence and temperature dependent [3]. It was also shown that in sequential or simultaneous He^+ – D^+ ion implantations D was trapped with He in the near surface region and D diffusion was limited only to the region where He was present [14]. While there are several attempts to explain the reduced blistering and reduced D retention, the actual cause for these observations remains unclear. One possibility for the reduced D retention is that implanted He might create a diffusion barrier for D transport [12]. Likewise, nano-sized bubbles might open-up additional pathways for D towards the surface thereby decreasing its transport into the bulk [13]. There is also a number of theoretical studies addressing the interaction between He and HIs. Density functional theory (DFT) calculations show strong attraction between He and HIs [9, 15], indicating preferential trapping of H around He clusters. Molecular dynamics (MD) simulations show that a large amount of H can be accommodated around He bubbles [16, 10, 17]. Increased D retention was observed experimentally in a recent study after thermal cycling of He irradiated W samples where visible bubbles were observed [18]. Increased D retention was found experimentally also in keV-range ion beam experiments [19, 20] which seems to be in contradiction to what was observed in mixed He-D plasma exposures. However, the challenge of these studies [19, 20] is that the applied He and D implantation energies cause displacement damage which is known to increase D retention in tungsten substantially. Therefore, one cannot distinguish unambiguously the influence of the presence of He from the displacement damage that the He creates.

At present it is still an open question how He affects HI retention in the bulk of tungsten. In order to test the hypotheses of He acting as a diffusion barrier and inducing preferential binding of HIs around He, we recently took an alternative experimental approach [21]. In order to decouple the influence of displacement damage created by He irradiation from the effect of the He-HI interaction, we performed a study with so-called self-damaged tungsten, by implanting 20 MeV

W ions into W creating displacement damage down to 2 μm to a damage level where D saturation is known to take place [22, 23]. In such a self-damaged W 500 keV He ions were implanted at 300 K which leads to a peaked He implantation depth profile at 0.84 μm depth according to a SRIM [24] calculation. This approach is in contrast to most of the studies of HI interaction where surface effects dominate the He-HI behaviour by simultaneous or sequential exposure to He and HI at low energy, see e.g. [2] and references therein. In that study [21] we have shown for the first time unambiguously in an experiment that D migrates and accumulates in the He implantation zone during annealing of a D saturated sample. D retention increased by a factor of two as compared to a non-He implanted highly self-damaged tungsten reference [21].

In this contribution D retention and transport is studied in He-implanted and self-damaged W by exposing it to D atoms at 600 K with atom energy of 0.28 eV and flux of about 3.5×10^{18} D/m^{2}s. We investigate how various He concentrations affect D retention. In a previous study it was shown that 1000 appm as implanted He at 300 K does not affect D retention in self-damaged W [25]. In the experiment presented herein, this finding will be tested for He concentrations larger by one order of magnitude. Finally, D retention in He implanted tungsten annealed to 1700 K will be studied in order to see how the expected evolution of microstructure influences D retention and transport as compared to the non-annealed He implanted self-damaged W.

2. Experiment

2.1 Sample preparation

In the experiment we used 12×15 mm^2 and 0.8 mm thick samples cut from a hot-rolled polycrystalline tungsten sheet with a purity of 99.997 wt.%. Grains are oriented parallel to the surface. Samples were mechanically and electro polished to a mirror-like finish [26] and then heated for 2 min in ultra-high vacuum at 2000 K for re-crystallization. This procedure enlarges the grain size to 10 – 50 μm [26, 27].

One half of the sample (referred as '*He*' half further on in the text) was irradiated by 500 keV He ions with a fluence of 14×10^{20} He/m^2 at room temperature (300 K) in the TOF beam line of the tandem accelerator at Max-Planck-Institut für Plasmaphysik (IPP), Garching [28]. Irradiation was performed by x- and y-scanning the He beam for lateral homogeneous implantation. According to SRIM [24], this leads to a He peak concentration of 6.8 at.% (68000 appm) in a depth of 0.84 μm

and a full width at half maximum (FWHM) of 0.3 µm. Moreover, with 500 keV He implantation displacement damage is created. According to SRIM a peaked damage profile is obtained with 1.2 displacement per atom (dpa) at the damage peak at a depth of 0.76 µm, as shown in Fig 4. Displacement damage was calculated by using a displacement energy of 90 eV [29] and evaluating the "vacancy.txt" output of the "Ion Distribution and Quick Calculation of Damage" calculation option of the SRIM 2008.04 code [24]. Two samples were also irradiated with smaller He fluences equal to 2×10^{20} He/m^2 and 7×10^{20} He/m^2 which is equivalent to 1 at.% He (10000 appm) and 3.4 at.% (34000 appm), in the peak maximum as calculated by SRIM, respectively. The corresponding maximum displacement damage doses are 0.17 dpa and 0.6 dpa for 1 at.% and 3.4 at.% He, respectively. Debelle et al. [30] measured with coincidence Nuclear Reaction Analysis (NRA) the depth profile of ^{3}He implanted with 500 keV energy to a fluence of 10^{20} He/m^2. The measured ^{3}He depth profile nicely coincided with the SRIM calculated profile in peak position, width and total fluence. We therefore can assume that the SRIM calculated He depth profile is a good approximation also for our conditions. The other half (referred further on in the text as '*no-He'* half) of the sample was covered during the He irradiation. This allowed us to expose both halves of each sample to D atoms at the same time, ensuring identical D exposure conditions for both. This allows a direct comparison of the results of D transport and D retention.

In some cases, as it will be explained in the next section, samples were additionally homogeneously irradiated by 20 MeV W ions to a fluence of 7.8×10^{17} W/m^2 at room temperature (300 K) in the TOF beamline [28] before or after the He irradiation. Using again a displacement energy of 90 eV and evaluating the "vacancy.txt" output of the "Ion Distribution and Quick Calculation of Damage" calculation option of the SRIM 2008.04 code [24] we create a displacement-damaged zone extending down to 2.3 µm with a peak damage level of 0.23 dpa at a depth of 1.35 µm [28]. Preceding studies with the same tungsten material and the same damaging procedure showed that D retention saturates for this damage level [22, 23].

2.2 Exposure procedure

To investigate the effect of He on D retention the samples were exposed to D atoms from a hydrogen atom beam source (HABS) at 600 K sample temperature in the INSIBA chamber at Jožef

Stefan Institute (JSI) [31][1]. In all measurements here the capillary was heated to a temperature of 2100 K. The average driving pressure measured in the gas supply side of the tungsten capillary was approximately 0.36 mbar with D_2. The flux hitting the sample was typically between 3-4×10^{18} D/m^2s. It was determined by exposing a plasma-deposited diamond like amorphous hydrogenated carbon (a-C:H) film on a Si wafer to D atoms at 600 K for 4 h. Measuring the resulting erosion crater by ellipsometry allowed us to deduce the incoming fluence of D given the known erosion yield of 0.017 C per incoming D [32, 33]. The large variation of the D atom beam flux is due to the fact that the D atom exposures on different samples were spread over two years. The D atom flux will be specified for each sample later on in the text. The D atom beam distribution was typically measured after the exposure series. One example of the D atom beam flux distribution is shown in figure 1. The a-C:H samples were 17x17 mm in size. In figure 1 the position and the size of a W sample is indicated (hashed area) together with the typical ^{3}He measurements positions for D depth profile analysis on '*He'* and '*no-He'* sides of the sample (grey squares).

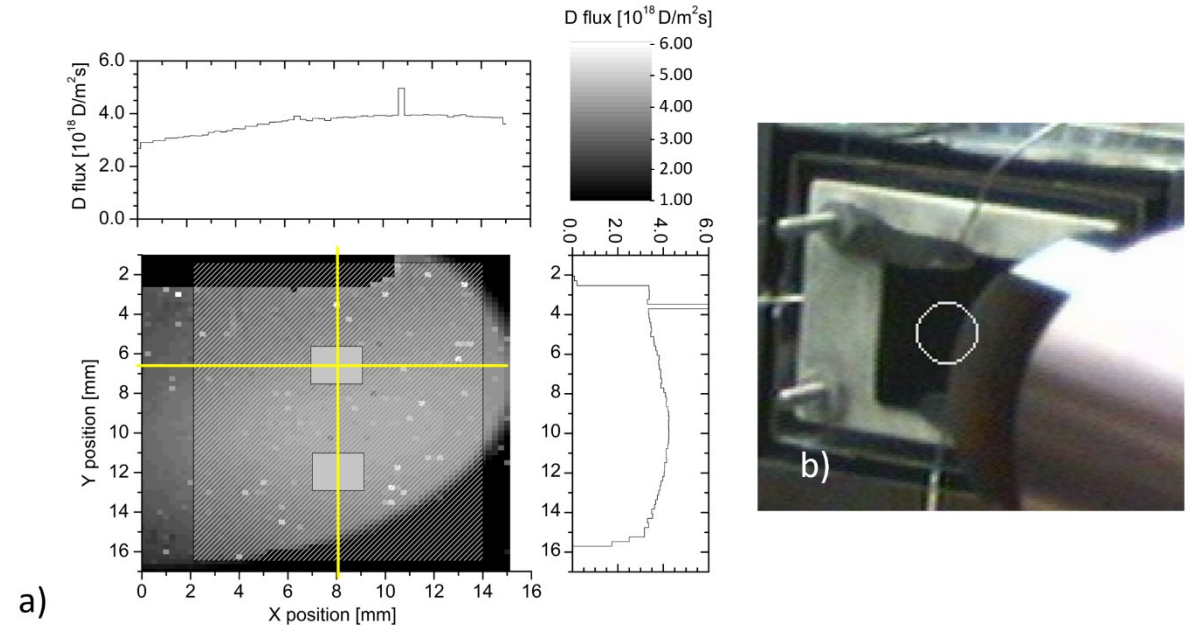

Figure 1: a) D atom flux density profile as obtained by ellipsometry from the erosion crater of an a—C:H sample after D atom exposure at 600 K for 4 h. The pictograms on the left and the top

[1] There is a mistake in the units of the driving pressure in this reference there should be 0.26 ± 0.01 mbar for D_2 and 0.2 ± 0.01 mbar for H_2.

show scans along the yellow lines. The hashed square shows the size and typical position where the W sample will be situated and the grey squares show ^{3}He measurements positions on 'He' and 'no-He' side and the size of the analysing beam. b) The picture of a-C:H sample mounted on the heater with molybdenum clamps, the thermocouples and the central ^{3}He ion beam position (white circle).

2.3 Analysis techniques

During as well as after the exposure to the D atom beam the D depth profile was measured by nuclear reaction analysis (NRA) utilizing a ^{3}He ion beam and the D(^{3}He,p)α nuclear reaction [34]. In order to obtain a D depth profile [35] the proton signal from the nuclear reaction was measured at six ^{3}He energies (730, 1040, 1550, 2570, 3390 and 4320 keV). Protons were detected by a 1.5 mm thick silicon detector (called NRA detector) positioned at 135° or 160° with respect to the incoming probing beam with a geometrical solid angle of 26.69 msr. The size of the probing beam was defined by two consecutive circular orifices of 2 mm in diameter positioned in the beam line. The beam impacts perpendicular on the sample surface. The depth resolution calculated by ResolNRA [36] for the two reaction angles are shown in figure 2. We can see that by changing the angle of the detector from 135° to 160° the depth resolution of the detection system improved as expected from [37]. At 160° this improvement is a factor of two in our case obtaining 200 nm depth resolution up to 1 μm depth and 400 nm above 1 μm depth. This improved depth resolution enabled us to detect the deuterium in depth in much better detail as compared to our previous study [21] as will be shown in the following figures. We also employed a detector to detect backscattered particles, the so-called RBS detector, located at 165° with respect to the incoming beam covering a solid angle of 0.689 msr. The signal from the RBS detector served us to measure the absolute dose of ^{3}He particles impacting on the sample. For one D depth profile, the proton energy spectra are first checked for energy calibration by SIMNRA [38] for all six measured energies. These six proton energy spectra are then all input into NRADC [39] that outputs the most probable D depth profile. The uncertainties of the obtained D concentrations in the depth profiles are due to statistical errors that stem from the limited amount of counts we measured at each measuring ^{3}He beam energy and by the uncertainty of the D depth profile fit by NRADC. Beside the statistical error we have also a systematic error of the NRA measurement due to NRA cross section determination (5 % [34]) and the accuracy in determining the accumulated dose equal to 5 % for our setup. For our accumulated charge conditions, the detection limit of the NRA is about 1×10^{-3} at. %.

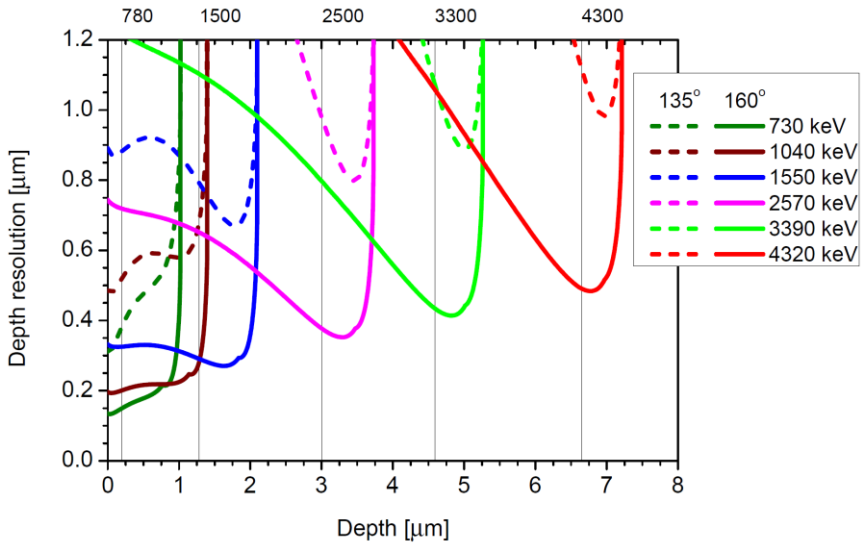

Figure 2: Depth resolution at the different ^{3}He energies calculated by ResolNRA [36, 38] *for 135° and 160° reaction angles of protons from the ^{3}He NRA nuclear reaction for our experimental conditions (sample detector distance 106.00 mm and circular shape of the detector with 19.54 mm diameter).*

When studying the influence of He on D transport and retention with ^{3}He as our analysing beam we need to make sure the ^{3}He beam fluence is small compared to the implanted ^{4}He fluence in the study. For one depth profile measurement we used the same collected charge for all six energies, where we used singly charged $^3He^+$ for the four low energies and $^3He^{2+}$ for the two highest energies. This results in 7.2 µC ion dose yielding 4.5×10^{13} He ions implanted for the four lower energies and 2.25×10^{13} He ions implanted for the two highest energies. Since our beam size is 2 mm in diameter this results in a fluence of 1.5×10^{19} He/m^2 and 0.75×10^{19} He/m^2, respectively. In order to compare this with the ^{4}He concentrations used in our study we calculated the implanted ^{3}He concentration depth profiles by SRIM. The results are shown in figure 3 for the six energies used for one D depth profile measurement. We can see that the implanted ^{3}He concentration is 0.08 at.% in the peak maximum for the lowest energy of 730 keV, creating 0.0089 dpa. The He concentration as well as the damaged dose decreases with increase of the analyzing beam energy. Therefore, compared to the studied ^{4}He concentrations, the ^{3}He concentrations for one depth profile are ten times lower than the smallest implanted ^{4}He concentration. We did change the position of the analyzing spot on the sample regularly. However, due to the sample size limitations

and variation of the D atom flux over the sample (fig. 1a), we had to use the same location more than once. From experience we can say that depending on the ^{4}He concentration or W-self-damage four to five measurements on the same analyzing position are still tolerable not to see an effect of the damage creation on the D retention in self-damaged W. This is why no more than five measurements were performed on the same analyzing position on any sample used in this study.

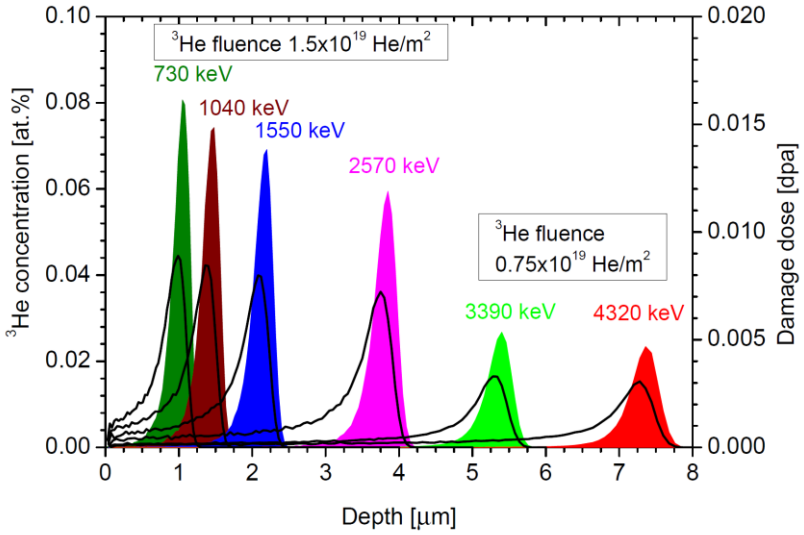

Figure 3: ^{3}He concentration depth profiles (filled curves) and damage depth distributions (black lines) as calculated by SRIM for the different analyzing ^{3}He energies and marked fluences used for one D depth profile measurement.

After the NRA measurements, the samples were cut into half with a diamond saw under water. After cleaning the samples in deionized water and ethanol thermal desorption spectroscopy (TDS) was performed on each half of the sample in order to measure the retained D amount and to investigate the kinetics of D desorption. The TDS was performed in the quartz tube of the TESS device at IPP [40]. Samples were heated by an oven heating ramp of 3 K/min up to 1010 K. The temperature response of the samples to the linear oven temperature ramp was measured during the ramp by a shielded thermocouple touching the sample surface. The desorbed gases were measured with a Pfeiffer/Inficon DMM 422 quadrupole mass spectrometer (QMS). We were recording 15 mass channels m/z = 1, 2, 3, 4, 12, 14, 16, 17, 18, 19, 20, 28, 32, 40, and 44 amu/q. Mass channels

above 4 amu/q showed no significant release of deuterium containing species. For the quantitative analysis the QMS signal for D_2 was calibrated after each temperature ramp with a calibrated leak bottle (Laco technologies) with a flow of 1.22×10^{14} D_2/s and a stated absolute accuracy of 4.6 %. The QMS cannot resolve He and D_2 meaning we could not distinguish between a possible desorption of He from desorbing D_2 during the TDS. In similar studies with 500 keV and MeV ^{3}He irradiated W [30, 25] no He desorption was observed up to 1770 K. Therefore, we assume that also in our case there is no He desorption from our samples during TDS.

Two of the samples with 6.8 at.% ^{4}He were heated to 1700 K for 30 min in vacuum by electron bombardment. The pressure during the heating was below 10^{-5} Pa.

Two samples, irradiated with 20 MeV W to 0.23 dpa and implanted with 500 keV ^{4}He to 3.4 at.%, were analysed by transmission electron microscopy (TEM) in Warsaw University, one as irradiated and one after annealing to 1700 K. TEM lamellas were prepared on the samples by conventional Focused Ion Beam (FIB) lift-out technique using a focused Ga^+ ion beam (Hitachi NB5000 dual-beam FIB-SEM). Rough milling was conducted at 40 kV and final thinning by low energy Ar plasma (0.6 kV). The thin lamella was investigated in a Hitachi HD2700 scanning transmission electron microscope (STEM) operated at 200 kV.

A third sample irradiated with 20 MeV W to 0.23 dpa and 500 keV He implanted also to 3.4 at.% ^{4}He was analysed at JSI by cross-section TEM (X-TEM) after annealing to 1700 K to investigate the possible He bubble production. To mitigate the artefacts induced by sample preparation it was prepared by combined mechanical thinning and low-angle Ar^+ etching [41]. The sample was investigated in a field-emission TEM (JEM-2010F, Jeol Inc.), operating at 200 kV. Micrographs were recorded by a slow-scan CCD camera (Orius SC1000, Gatan Inc.).

3. D retention results

3.1 6.8 at.% He irradiated W sample

We first consider a sample that was only irradiated by He. The sample was irradiated by 500 keV ^{4}He at 300 K to a calculated ^{4}He concentration of 6.8 % in the peak maximum (referred further on in the text as '*6.8 % He'* sample) and then exposed to D atoms with a flux of 3.8×10^{18} D/m^{2}s at 600 K. Nuclear Reaction Analysis at different exposure times allows to derive the D depth profiles shown in figure 4. The proton detector was at this exposure positioned at the reaction angle of 160°. In the figure we also show the damage dose depth profile as created by

500 keV ^{4}He irradiation and the ^{4}He depth profile, both calculated by SRIM. After 3.5 h the D atoms penetrate to a depth of about 300 nm not reaching yet the He zone. With further exposure the D atoms penetrate further into depth occupying also the He zone. Between 83 h and 132 h of D atom exposure (total fluence of 1.1 and 1.8×10^{24} D/m^2, respectively) D concentration stays unchanged beyond 1 µm but slightly increases in the depth between 0.5 µm and 1 µm. The final D depth profile very much resembles both the damage depth profile and the ^{4}He implantation depth profile. The position of the maximum D concentration of (1.1 ± 0.07) at.% coincides with the position of the maximum displacement damage and/or with the maximum implanted ^{4}He concentration (The limited depth resolution does not allow to differentiate between the two). This value is by a factor of three times larger than the typical D concentration of (0.35 ± 0.2) at.% observed in our self-damaged W samples for the same exposure conditions (20 MeV or 10 MeV W-ion irradiation to damage dose levels where damage saturation is observed and exposure to D atoms at 600 K at similar D atom flux) [31, 42]. This comparison clearly indicates that either He influences the evolution of the radiation damage during the implantation or He itself has a significant trapping effect on the D atoms later in the atom loading.

During the D atom exposure NRA was also performed on the *'no-He'* half of the samples. As expected, D uptake was very small. One depth profile after 24 h exposure is shown in figure 4. At the surface we derived an areal density of 0.7×10^{19} D/m^2 which is attributed to surface adsorption [43]. The exact concentration cannot be determined due to the limited depth resolution at the surface. Deeper in the bulk of the sample, a constant D concentration of 8×10^{-3} at.% was derived, which is the same concentration level as observed on the 'He' irradiated side beyond 2 µm. This can be attributed to D retention due to natural defects present in the sample. Uptake and retention of the un-irradiated tungsten can therefore be neglected compared to the irradiated case for this study.

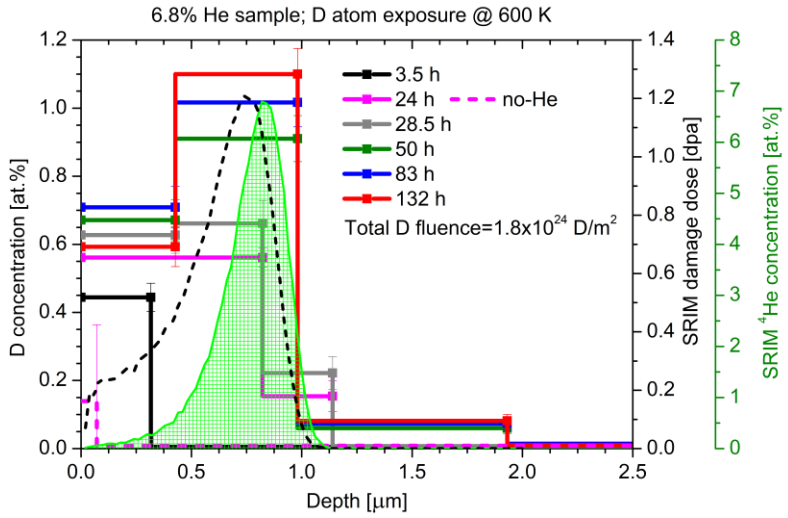

Figure 4: D depth profiles as measured by NRA at different D exposure times for the '6.8 % He' W sample irradiated with 500 keV He ions to a of fluence 1.4×10^{21} He/m^2. Sample was exposed for 132 h to D atoms at 600 K to a flux of 3.8×10^{18} D/m^{2}s, yielding a total fluence of 1.8×10^{24} D/m^2. D depth profile for 'no-He' side for 24 h hours exposure is also shown as dashed line. SRIM calculation of ^{4}He concentration depth profile (green hashed area) and damage dose (black dashed line) induced by He irradiation is also shown, right scales.

3.2 Different He concentrations in He and W irradiated W samples

In order to further elucidate the effect of different ^{4}He concentrations on D retention in W and to be able to resolve the effect of the presence of He itself from the effect of displacement damage on D retention we followed the sample preparation procedure according to our previous work in [21] for studying the accumulation of D in the He implantation zone. This means samples were first irradiated by 20 MeV W ions, then exposed to 10 eV/D plasma at 300 K to populate the defects and only then half of the sample was irradiated by 500 keV ^{4}He. The samples were then step wise annealed to 800 K as is described for the *'3.4 % He +W dam'* sample in [21]. Complete desorption of deuterium was achieved after annealing at 800 K, as measured by NRA for all the samples from this subsection. Only after this procedure the samples were exposed to the D atom beam for the present study. With the fact that we annealed the sample up to 800 K one could expect some reduction of radiation damage due to annealing [44]. One could also expect some influence of D presence on damage creation during He irradiation [42, 45]. We will discuss these issues along with the results. The samples from this subsection will be later on referred as *'He + W dam'*.

We will first present results for the sample which was irradiated by 500 keV He ions to a fluence of 1.4×10^{21} He/m^2, referred further on in the text as '*6.8 %He + W dam'* sample. The whole sample was exposed to D atoms with a D atom flux of 4.1×10^{18} D/m^{2}s for 70 h yielding a D fluence of 1.0×10^{24} D/m^2. In figure 5a we show the D depth profiles measured on both halves of the sample at different exposure times and the final D depth profile obtained after 70 h. In this case the detector position was at 135^o meaning the depth resolution was worse than in the case of the depth profiles shown in figure 4. D was slowly penetrating into the bulk of the material reaching after 18 h 0.8 μm, after 22.5 h 1.15 μm and after 70 h populating all the defects induced by He and W ion irradiation down to 2 μm. Already during the exposure the D concentration was always higher on the *'He'* side as compared to *'no-He'* side down to a depth of 1 μm. The penetration depths are very much similar on both sides of the sample. In figure 5b we show the final D depth profiles for '*He'* and *'no-He'* side of the '*6.8 % He + W dam'* sample together with the He implantation depth profiles and displacement damaged dose as calculated by SRIM. As can be observed we obtain a maximum D concentration of 1.08 at.% at the depth where the He was implanted. Beyond the He implantation zone down to 1.9 μm, we obtain a constant D concentration of 0.37 at.%. Comparing the D depth profile to the one obtained on the '*no-He'* side of the sample the agreement in D concentration at depths beyond 1 μm depth is excellent being also 0.37±0.3 at.%. There only W irradiation affects D retention. This concentration is in agreement with our previous measurements on 20 MeV W ion irradiated W samples exposed to D atoms at 600 K obtaining also 0.37±0.2 at.% [46]. As mentioned above, one could expect a reduction of D concentration by 15 % [44] due to the defect annealing expected at 800 K but by comparing to our previous studies [46] the reduction of D concentration is not clearly observed and is probably hindered to some extent due to the presence of D during the annealing [47]. In figure 5b we also show for comparison the 132 h D depth profile for '*6.8 % He' sample*, already shown in figure 4, where no additional W irradiation took place. The D depth profile measured on the *'He'* side of the '*6.8 % He + W dam'* sample is down to 1 μm almost identical to the D depth profile obtained for '*6.8 % He'* sample. This comparison indicates two things. Firstly, the additional damaging induced by W ions did not change the D depth profile and especially the total concentration in the He zone. This also means that the presence of D during the He irradiation did not have significant effect. Moreover, due to the fact that D diffused beyond the He zone and we obtained good agreement with our previous measurements for the D concentration in larger depth

where only W damaging was present, we believe that the defects were completely populated already at a fluence of $1x10^{24}$ D/m^2. Secondly, the D retention from the surface to about 0.3 μm is increased presumably due to the presence of He close to the surface. The increase cannot be attributed to a larger damage dose induced by ^{4}He irradiation for the following reason: Saturation of D concentration after plasma exposure was observed for damage doses above 0.2 dpa [22, 23]. We can confirm this saturation also for our 600 K D atom exposed samples. In another experiment we damaged W samples by 10 MeV W ions to a damage level of 0.5 dpa and we obtained at maximum D concentration of (0.33 ± 0.2) at.% [42] which is (within the error bars) in good agreement with the D concentration of the sample damaged by 20 MeV W ions with a damage dose of 0.23 dpa, shown in figure 5 and in [31, 46]. The damage dose at the surface is 0.13 dpa and increases up to 0.6 dpa at 0.3 μm for '*6.8 % He + W dam*' sample therefore we are all the time in damage saturation and the effect of the displacement damage alone would account for 63 % of D concentration observed there.

From this comparison of the W irradiated, He irradiated and W+He irradiated samples we conclude that the increase in D concentration at the depth between 0.5 and 1 μm is due to the influence of the presence of He. We observe an increase in D concentration at the maximum of the He concentration by a factor of 2.9, as calculated by dividing the maximum D concentration in that zone (1.08 at.%) by 0.37 at.%, which is the D concentration obtained on the only W irradiated half of the sample, the *'no-He'* side.

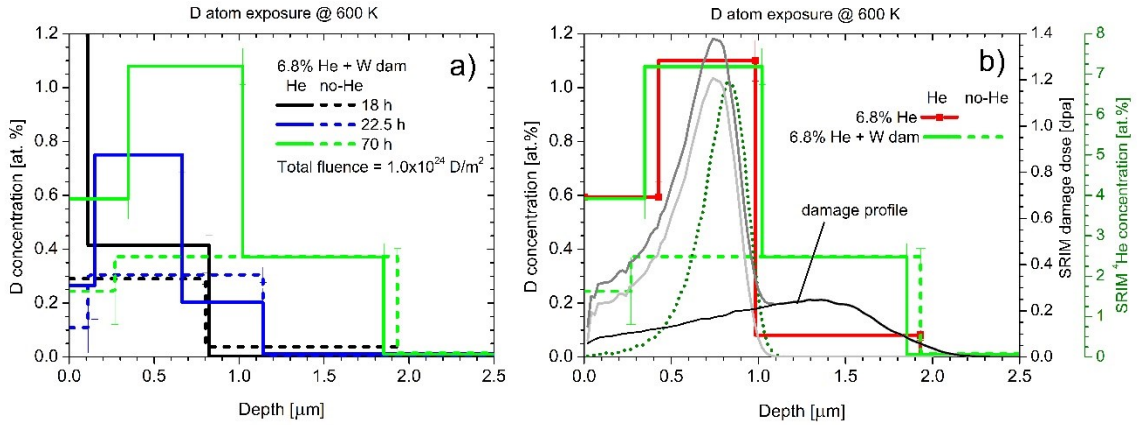

Figure 5: a) The D depth profiles measured at different times on the 'He' and 'no-He' side of the '6.8 % He + W dam' sample. On the 'no-He' side only W irradiation was performed. The sample was exposed to D atoms at 600 K to a flux of 4.1×10^{18} D/m^{2}s yielding a final fluence of 1.0×10^{24} D/m^2 after 70 h of exposure time. b) Comparison of the final D depth profiles (left scale)

measured on the 'He' side and 'no-He' side to the final D depth profile on the '6.8 % He' sample from figure 4 is shown. Calculated damage dose for the He implantation (light grey line), the W implantation (solid black line), and the sum (grey line) are shown (right scales). Calculated ^{4}He concentration is shown in addition as green dotted line.

In order to study the effect of different ^{4}He concentrations on D retention we performed the identical experimental sequence as for the '*6.8 % He + W dam*' except that two different implanted He fluence were used: 2×10^{20} He/m^2 on one sample and 7×10^{20} He/m^2 on a second sample. This corresponds to an implanted concentration of 1 at.% He (10000 appm) and 3.4 at.% (34000 appm) in the peak maximum as calculated by SRIM and shown in figure 7a, respectively. Also in these cases only half of each sample was irradiated by He and the other half served as He-free reference, irradiated only by W ions. Moreover, the same D plasma exposure and stepwise annealing procedure to 800 K of D filled sample was performed on the two samples as described above and then D atom exposure at 600 K was performed. In the case of the 3.4 % He sample the D atom exposure flux was 3.8×10^{18} D/m^{2}s and exposure time was 96 h yielding a fluence of 1.3×10^{24} D/m^2. The 1 % He sample was exposed to D flux of 3.5×10^{18} D/m^{2}s for 120 h yielding a fluence of 1.5×10^{24} D/m^2.

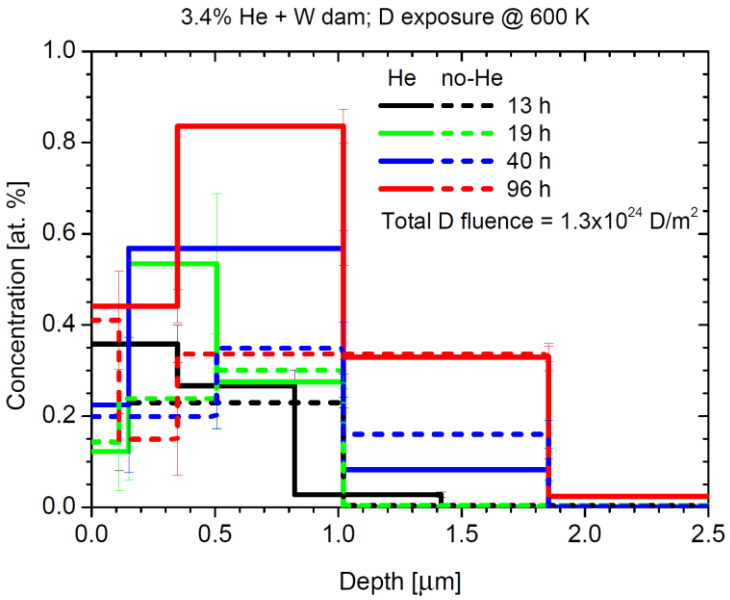

Figure 6: D depth profiles measured on '3.4 % He + W dam' sample at different exposure times. The sample was exposed to D atoms at 600 K with an exposure flux of 3.8×10^{18} D/m^{2}s and with the total exposure time of 96 h yielding a fluence of 1.3×10^{24} D/m^2. The D depth profiles for the 'no-He' side for each exposure time are also shown (dashed lines).

For both samples the D depth profiles during the D atom exposure were measured as was the case shown in figure 5a for the '*6.8 % He + W dam'* sample. As a second example we show in figure 6 the D depth profiles measured on the '*3.4 % He + W dam'* at different exposure times. D was slowly penetrating into the bulk of the material reaching after 13 h 0.8 μm, after 19 h 1 μm, after 40 h 2 μm and after 96 h D atoms populate all the defects induced by He and W ion irradiation down to 2 μm. The penetration depths are very much similar on both sides of the sample but higher D concentration was observed on the *'He'* side as compared to *'no-He'* side, as was the case for the '*6.8 % He + W dam'* sample. Also the penetration depths are similar for similar exposure times for the two samples shown in figures 5a and 6. Similar trend is observed for the '*1 % He + W dam'* and for this reason we do not show these data since it would have the smallest effect. In all three cases, slow penetration of D into the sample was observed, populating the defects in the He zone and at the same time further proceeding into the no-He zone where only defects due to W ion irradiation were present. Comparing the moving diffusion front of D on the *'He'* side and '*no-He*' side for all the studied samples, we get the same rate of uptake, meaning He does not act as a diffusion barrier. We assume that in all cases the D fluences were high enough to populate all the defects, which is confirmed by the fact that the damage layer created by the 20 MeV W irradiation beyond the He implantation zone is completely saturated down to 2 μm. Exposing He and/or W irradiated samples to higher D fluences, does not influence the amount of retained D, as retention is only limited to the He + W implanted zone.

The final D depth profiles as measured by the proton detector at a reaction angle of 135° on the three samples with different He concentrations are shown in figure 7a. For the *'6.8 % He + W dam'* and *'3.4 % He + W dam'* samples, these are the same data as in figures 5a and 6, respectively, at the final exposure times. The D depth profiles and D concentration measured on the '*no-He'* sides of all samples agree very well, within the error bars, obtaining 0.34±0.2 at.% for the two samples with smaller He concentration. Meanwhile, on the *'He'* side we can observe a clear difference between the samples with different He concentrations. Focusing on the D concentration at the depth that corresponds to the maximum implanted He concentration, a small increase in D concentration compared to the W irradiated can be observed for the 1 % He sample obtaining 0.49 at.%. With higher implanted He concentration also the concentration of D drastically increases. For the *3.4 % He* sample we measured a D concentration of 0.84 at.%. By

dividing the D concentration measured on the only W irradiated side with the maximum D concentration measured between 0.5 µm and 1µm on the *'He'* side we obtain a factor of 1.4 for 1 % He, a factor of 2.5 for the 3.4 % He and 2.9 for the 6.8 % He sample, which was already calculated above.

Assuming that both effects add up independent from each other we can calculate the D retention that is the consequence of the presence of ^{4}He and not due to the displacement damage from the D depth profiles shown in figure 7a. In figure 7b we plot the difference in D amount on the *'He'* side subtracted by the D amount on the *'no-He'* side down to 2 µm from figure 7a as a function of He fluence. We can see that the additional D retention increases almost linearly with the increase of He fluence. We get a D over He ratio of 0.29±0.2 when we make a linear fit through the data points. This shows that at small He concentrations, below 10000 appm, the possible effect of He inclusion on D retention is very small, being below 6×10^{19} D/m^2. This agrees with the study of Markina et al. [25] who found no influence of He implantation in self-damaged W on D retention for He concentrations of 1000 appm.

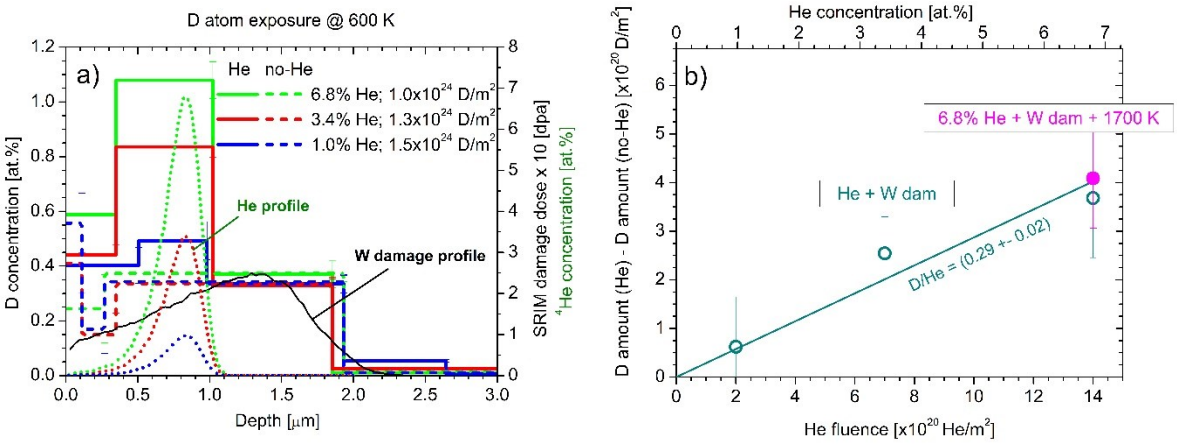

Figure 7: a) D depth profiles measured for 'He + W dam' samples with different He concentrations after the exposure to D atoms at 600 K (solid lines). The D depth profile for the 'no-He' half for each sample is also shown (dashed lines). The ^{4}He concentration depth profiles (dotted lines in respective colours) and W damage depth profile (black line) are shown as calculated by SRIM in addition – right scale. b) The D retention from 0 to 2 µm obtained on the 'He' side on the 'He + W dam' samples as a function of He fluence corrected for the retention found in the 'no-He' halves. The retention obtained on the '6.8 % He + W dam + 1700 K' sample is also shown for comparison, magenta data point. Linear fit (cyan line) to the data is shown including the data for the annealed sample, obtaining a ratio of D/He = 0.29.

3.3 D retention in 1700 K annealed He samples

From the literature one can expect that when a W sample irradiated by W ions is annealed up to 1673 K the majority of the defects are annealed [48]. This means that most of the defects responsible for the increase in the D retention beyond the He implantation zone should be gone and we should observe very little D retention. Little is known about D retention in He implanted and annealed tungsten. It was shown in literature that when one anneals a He containing W sample no He is released after thermal treatment up to 2000 K [25, 30]. This is explained by the high de-trapping energy that is necessary to release He from a vacancy or vacancy cluster to which it gets bound during the implantation [9, 49]. After such high temperature annealing it was shown that He starts to agglomerate forming larger He bubbles [50]. Moreover, according to a study by Chernikov [50] the size of He bubbles formed in the bulk of W depends mainly on the annealing temperature and not so much on the He concentration. Chernikov used two types of W specimens. The first specimens were W polycrystals implanted with He energy between 0 and 12 MeV to reach a constant concentration of 600 appm. The second specimens were [001] W single crystals where He was introduced by irradiation with 40 keV He ions creating a peaked profile and concentrations of few at.%. After the He irradiation samples were annealed to various temperatures for 1 h. For both types of He implantations it was observed that He starts to agglomerate into visible bubbles above 1523 K and after annealing at 1673 K He bubbles of few nm in radius can be observed by TEM [50].

In the present study the sample that was above presented as '*6.8 % He + W dam'* sample was, after the D atom loading, NRA analysis and TDS, annealed at 1700 K for 30 min in ultrahigh vacuum. We refer to this sample then as '*6.8 % He + W dam + 1700 K'* sample. This annealed sample was again exposed to D atoms at 600 K and the D depth profiles during the exposure were derived with NRA. The NRA detector was positioned in this case at a 160° reaction angle. The mean D atom flux at the analysing position was determined to be 3.2×10^{18} D/m^{2}s. The D depth profiles measured at different exposure times are shown in figure 8. The first D depth profile was measured after 24 h of exposure and we can see that D penetrated into the sample and got trapped exactly where He was implanted. With further increase of D exposure time (48 h and 74 h) the D atom concentration grew only in the He zone. Between 74 h (8.6×10^{23} D/m^2) and 168 h (1.9×10^{23} D/m^2) of D exposure, D concentration increased from 0.5±0.40 to 1.36±0.10 at.% but did then not increase any further up for 190 h. Unfortunately, we did not perform a measurement

in between 74 h and 168 h, so the exact exposure time when saturation occurred cannot be determined. The obtained final maximum D concentration of 1.35 at.% is 3.6 times higher as compared to D concentration of 0.37 at.% in self-damaged W. Outside of the He peak, D retention in this half of the sample is very small at all exposure times even though the sample contained damage up to 2 μm due to W irradiation initially before annealing at 1700 K. We show also the final D depth profile on the *'no-He'* half where we see very similar retention values than outside the He peak of the He half. Here a rather homogeneous D concentration down to 1.8 μm is observed coinciding with the range of the initial 20 MeV tungsten damage. The concentration of 0.076 at.% is 20% of the initial D concentration of 0.37 at.%, meaning that, as expected, most of the displacement damage was removed due to annealing to 1700 K. Very recent investigations by Zibrov et al. [51] with single crystals confirm this low retention. This means in summary, that with the annealing the He containing half of the sample did not loose its capacity to store deuterium as was the case for the displacement damage.

In figure 8 we also show the final D depth profile obtained on the non-annealed '*6.8 % He'* sample (just He irradiated as shown in figure 4) to compare it to the D depth profiles obtained after annealing. Interestingly, even though the D depth profile measurement was performed with the same experimental settings (NRA detector at 160°) as for the '*6.8 % He'* sample, a less peaked proton spectrum was measured for the non-annealed sample indicative for a wider D concentration at a depth of 1 μm. As discussed above, deconvolution of the measured proton spectra reveals a local D concentration of 1.35±0.10 at.% compared to 1.10±0.07 at.% for the non-annealed sample. Together with the observation from above that the displacement damage was mostly annealed out this different width in the D profile must reflect a different width of the He profile. Hence, He must have probably agglomerated into a narrower region. Such agglomeration of He was indeed also measured by Debelle et al. [30] after annealing a He implanted sample at 1773 K. The final total D amounts down to 1.93 μm of both samples are very similar. For the '*6.8 % He'* sample being $(59\pm5)\times10^{19}$ D/m^2 as compared to $(49\pm6)\times10^{19}$ D/m^2 for the annealed sample. The total D amount for the '*6.8 % + W dam + 1700 K'* sample is also plotted in figure 7b with the D amount obtained on the '*no-He'* side down to 2 μm subtracted. The retained amount in the D peak which is attributed to be due to the He only is similar to the D retained amount obtained on the non-annealed '*6.8 % He + W dam'* sample. The obtained linear fit with D over He ratio of 0.29 ±0.2 is obtained for all the data points shown in figure 7b. This means in summary, that despite the 1700 K

annealing that expectedly caused substantial change in microstructure the retained He did not change its capacity to store deuterium.

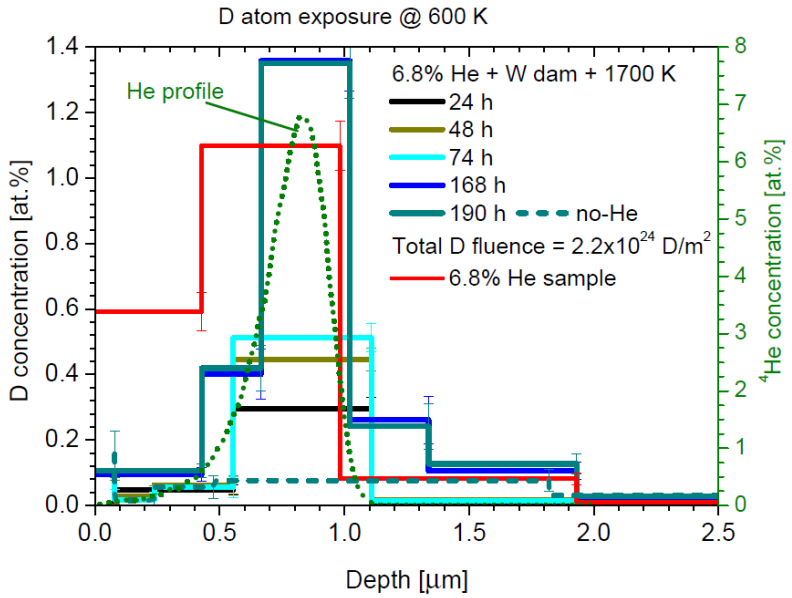

Figure 8: D depth profile measured for the '6.8 % He + W dam' sample that was annealed at 1700 K for 30 min and afterward loaded by D atoms at 600 K. The sample was exposed for 190 h to a mean D atom flux of 3.2×10^{18} D/m^{2}s, yielding a total fluence of 2.2×10^{24} D/m^2. For comparison we also show the final D depth profile on 'no-He' side and measured on the as implanted, '6.8 % He' sample, that was previously shown in figure 4 (red line). The NRA reaction angle was 160^o.

Based on the work of Chernikov [50] we expect that due to the annealing at 1700 K He bubbles exist in a depth of 1 µm in the '*6.8 % He + W dam' half* of our sample. In order to further study the possibility of such a He bubble layer acting as a permeation barrier we also annealed the '*6.8 % He'* sample to 1700 K for 30 min and after this the sample was irradiated by 20 MeV W with the same irradiation conditions as for the previous samples. We refer to this sample then as '*6.8 % He + 1700 K + W dam'* sample. This additional damaged layer beyond the He serves us as an indicator for penetrating D into depth by measuring the trapped D at the formed defects. The sample was exposed to a D atom flux of 3.2×10^{18} D/m^{2}s at 600 K and the obtained D depth profiles during the exposure are shown in figure 9 after 4, 22, 28, 46, 70, 97 and 168 h. In all cases we

show also the *'no-He'* counterpart as dashed lines being exposed to similar D flux as the '*He*' side. D slowly penetrated into the bulk reaching after 22 h a depth of 1 μm with D concentration between 0.3 and 0.4 at.%, see figure 9a. With further exposure time D concentration started to increase locally, figure 9b, as was the case also for the sample in figure 8. However, even though the D concentration increased locally where He probably agglomerated, D transport proceeded also further into the bulk. After an exposure time of 97 h (figure 9c) D atoms reached and saturated also the whole W damaged zone. However, with an additional 70 h exposure the D concentration still increased locally where He was implanted (figure 9d). After a total of 168 h of exposure yielding a fluence of 1.9×10^{24} D/m^2, the D concentration in the He implanted area saturated and the D depth profile did not change with additional 115 h of exposure (total exposure time of 283 h) as can be seen in figure 9d. We can see that for most cases the D front on the *'He'* side moved with the same speed further into depth as in the *'no-He'* side. This means that the He layer did not act as a permeation barrier slowing down or even preventing D from further transport into the depth. The maximum D concentration in the He zone was 1.7 at.% which is close to the sum of the maximum D concentration obtained on the annealed '*6.8 % He + W dam + 1700 K'* sample, obtaining 1.35 at.% (figure 8) and the D concentration obtained due to 20 MeV W ion damaging. The D retention in the '*no-He'* side reached a saturation D concentration of 0.44 at.% after 168 h of D exposure. This is higher as compared to D retention on the '*no-He'* side for '*He + W dam'* samples shown in figure 7a obtaining 0.35-0.37 at.%. This lower D concentration of samples from figure 7a can be explained by the annealing of samples up to 800 K before the D atom exposure, which results in the annealing of defects [44].

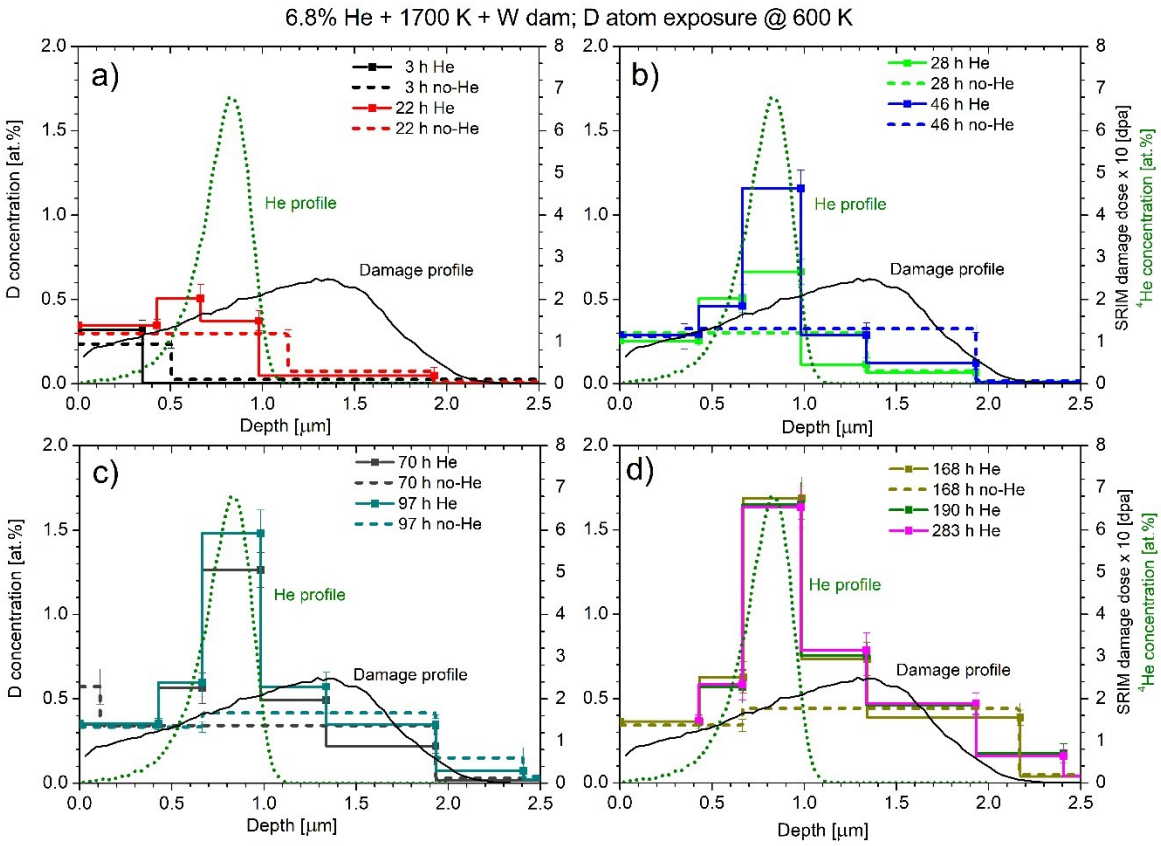

Figure 9: D depth profiles (left scales) measured at different times of D atom exposure with a flux of 3.2×10^{18} D/m^{2}s at 600 K for the '6.8 % He + 1700 + W dam' sample. D depth profiles measured on the 'no-He' half are also shown. Calculated ^{4}He concentration depth profile and W damage dose are shown in addition (right scales).

3.4 Thermal desorption spectra

After the NRA analysis, the samples were cut into half to be able to perform thermal desorption spectroscopy on the *'He'* and *'no-He'* halves independently. Cutting was conducted with a water-cooled diamond blade so that no deuterium was released during the process. We show on figure 10 the D desorption spectra for four specimens, for the *'6.8 % He'* sample (D depth profiles shown in figure 4), the *'He' side* of the *'6.8 % He + W dam'* sample (D depth profiles shown in figure 5) and for both halves of the *'6.8 % He + 1700 K + W dam'* sample (D depth profiles shown in figure 9d). In the case of *'6.8 % He'* sample, the sample was not cut into half before TDS, since the contribution from the *'no-He'* side was assumed to be small, which is from the measured D depth profiles on figure 4 accounted to be less than 10%. The D desorption

spectrum for this sample shows a single desorption peak centred at 770 K. The D desorption spectrum on the He half of the '*6.8 % He + W dam'* sample shows also a single desorption peak but with a shift in a peak position to 800 K. The peak height is higher and broader. This can be accounted to the additional D retention due to 20 MeV W ion irradiation creating additional damage down to 2 µm. We also show the D desorption peaks for the '*He*' and the *'no-He'* sides of the '*6.8 % He + 1700 K + W dam'* sample. We can see that both D desorption spectra show the same peak profile and peak position is as in the case for the '*6.8 % He + W dam*,' only the peak intensity is higher for the *'He'* side and lower for the '*no-He*' side. The difference between the *'no-He'* and the *'He'* side of the '*6.8 % He + 1700 K + W dam'* sample is due to the additional D retention around implanted He where He bubbles were created due to annealing. Comparing the *'He'* sides of the '*6.8 % He + W dam'* and '*6.8 % He + 1700 K + W dam'* samples we see a 8% reduction in peak height. This difference we attribute to the stepped annealing to 800 K of the '*6.8 % He + W dam'* sample before the D exposure which reduced the amount of damage as compared to '*6.8 % He + 1700 K + W dam'* where sample was annealed to 1700 K after He irradiation and only after this W ion irradiation took place. This little change in peak height is another proof that irrespective of being annealed or non-annealed, a sample implanted initially with He does not change its capacity to store deuterium.

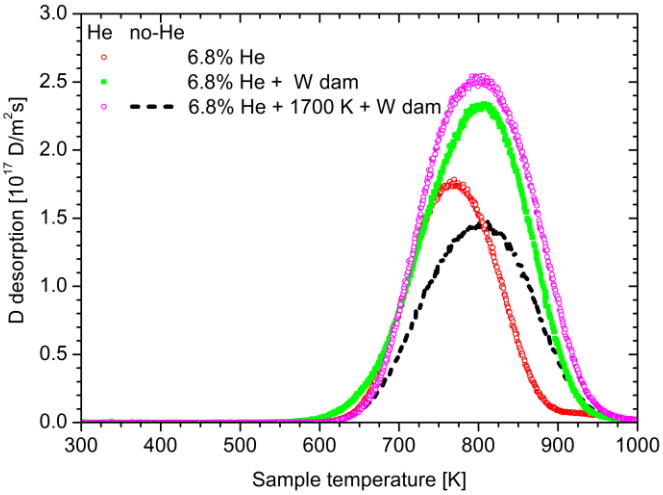

Figure 10: Thermal desorption spectra obtained on the '6.8 % He' sample (D depth profiles shown in figure 4), the 'He' side of the '6.8 % He + W dam' sample (D depth profiles shown in figure 5) and on both halves of the '6.8 % He + 1700 K + W dam' sample (D depth profiles shown in figure 9d).

4. TEM analysis

Two samples irradiated with W ions up to 0.23 dpa and 3.4 at.% He were further analysed by STEM. One sample was as irradiated (Figure 11a) and one after annealing to 1700 K (figure 11b, 11c). The as irradiated sample shows a characteristic double-layered structure, induced by implantation of W and He ions at different implantation energies, and therefore implanted at different depths. The visible damage of the 20 MeV tungsten ions reaches a depth of approximately 2.1 μm while the microstructural change of the 500 keV He ions are concentrated around 0.8 μm. The ion accumulation zones correspond to two thick black zones, indicative for a large density of radiation-induced defects (Figure 11a). The variation of the contrast in the whole implantation zones indicates extensive structural damage of the host material. After the annealing, significant reduction and aggregation of small defects and rearrangement as well as partial healing of dislocations can be observed, with dislocations remaining in the He zone between 0.68 and 0.92 μm (figure 11b). This nicely corresponds to the width and the peak position of the SRIM calculated He depth profile, shown in figure 4. In the same sample, when there is no He present in the structure (*'no-He'* side), the dislocations almost disappear upon annealing and only few dislocation lines are observed within a damage depth of 2.2 μm, which corresponds to the initial W self-damaging depth (figure 11c). In general, after the annealing - when the sample is observed in [100] zone axis - when He is present in the structure the remaining dislocations tend to form edge-on a⟨100⟩ dislocation loops networks, while the sample without He the remaining defects are mixed populations of line dislocations and dislocation loops with Burgers vector of either $a\langle 100\rangle$ (strong, straight, edge-on line segments and faint faceted circles) or $a/2\langle 111\rangle$ (open ellipses). Apparently, upon annealing, vacancy clusters that formed under W-ion irradiation become thermally unstable (mobile) and partial healing of dislocations can be observed, while interstitial loops start to change their shape and eventually annihilate. This is significantly supressed by the He presence. Here larger dislocation loops with larger density and the preservation of the dislocations after annealing was observed compared to *'no-He'* side. This is in line with observations in literature where the presence of He in the bulk of tungsten can critically influence the brittleness and the mechanical behavior of the tungsten bulk, as the strength parameter (critical resolved shear stress) has been found to be dependent on the Burgers vector and geometry of the dislocation loop with respect to the gliding dislocation [52].

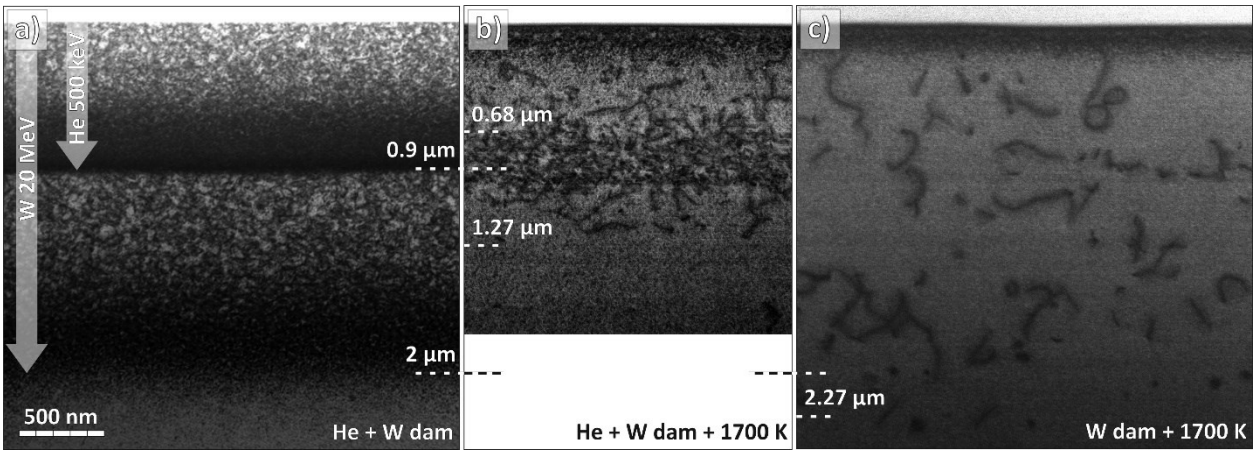

Figure 11: STEM micrographs of lamella cuts out of W samples irradiated with 20 MeV W ions with a fluence of 7.8×10^{17} W/m^2 yielding a calculated damage dose of 0.23 dpa at the beam maximum and 500 keV He ions with a fluence of 7×10^{20} He/m^2 obtaining 3.4 at. % of He in the peak maximum. a) as implanted and annealed at 800 K, b) and c) after annealing at 1700 K. The 'He' side in b) showing a dislocation network in the He-rich zone. The 'no-He' side in c) only large dislocation loops with either a/2⟨111⟩ or a⟨100⟩ Burgers vectors are visible.

The nano-sized defects, like voids or bubbles, induced by implantation and modified by post-annealing, can be directly imaged using TEM when they are larger than ≈ 1 nm. Due to lack of contrast of the small He bubbles we used a combination of bright field (BF) TEM images in under- and in-focus, exploiting the Fresnel contrast for their visualization. The cross section TEM analysis of a post-annealed sample revealed numerous voids concentrated about 1 µm from the sample surface (figure 12). We assume that the observed voids are the He bubbles. The in-focus (figure 12b1) and defocused (figure 12b2) micrograph pairs were used to determine their precise size and distribution. The size distribution of the He bubbles in the matrix and on the grain boundaries (GB) do not differ significantly (figure 12e1 & 12e2), however the visualization of the He bubbles on the incoherent grain boundary can be challenging due to partial grain overlapping. The mean radius of the He bubbles obtained on the inspected sample area is 1.5 nm averaged over N=176 bubbles found, while on the GB the mean bubble size is 1.4 nm being averaged over N=25 bubbles.

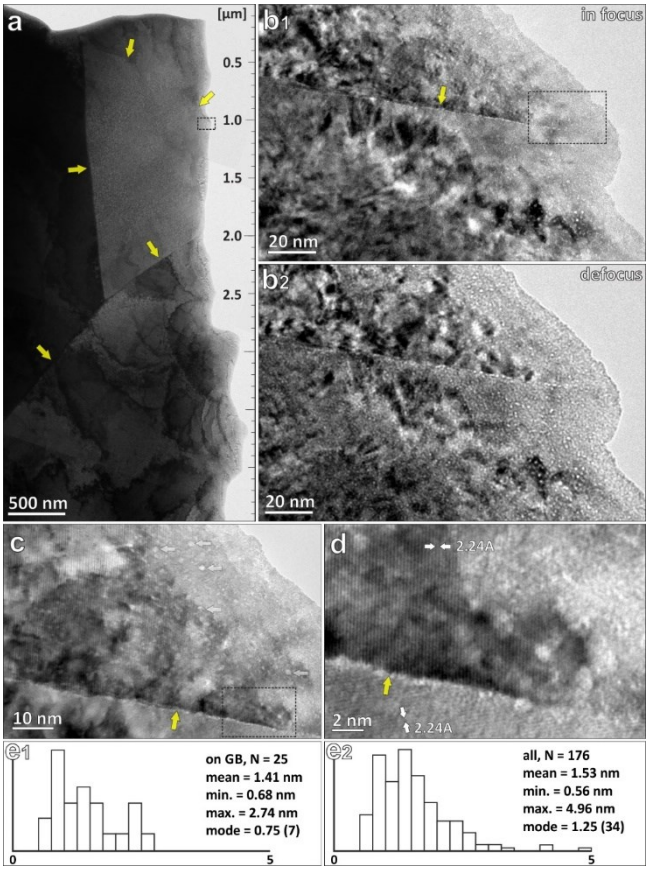

Figure 12: TEM micrographs of a cross-section of an identical tungsten sample as shown in figure 11 b and c with different magnification; Implantation direction is from top towards bottom. Yellow arrows mark the grain boundaries. The small rectangle in a) marks the region further analysed in b1) and b2) which show high resolution-TEM micrographs of the implanted region (b1) in-focus and (b2) at 1.2 µm defocus to enhance the contrast of the voids which we consider to be He bubbles. The small rectangle in b1) marks the region with higher magnification shown in c) and the rectangle in c) is further magnified in d). The distribution of bubbles in the matrix and near grain boundaries is uniform (c). Detailed analysis of the thin region near incoherent grain boundary, revealed numerous nano-sized voids (d). The size distribution of the voids (He bubbles) on the grain boundary (e1) and in the matrix (e2) do not show significant difference (N = number of voids measured, mean = central value, average; mode = value that appear most often).

5. Modelling

Modelling of the experimental results was done using the MHIMS-R code [53], which is an 1D rate-equation code that employs the fill-level dependent deuterium-defect interaction picture. The modelling was done for the '*6.8 % He + 1700 K + W dam'* sample, where He bubbles were observed and for the '*6.8 % He'* sample. This so-called fill-level model is based on density

functional theory (DFT) calculations which show, that the de-trapping energies of HIs depend both on the defect type and on the number of HI that are trapped in the same defect. This was shown to be valid for both vacancies [54] [55] [56] and for vacancy clusters [57].

To use the MHIMS-R code, also the surface boundary conditions have to be defined. As the D atoms impacting the surface had an energy of only 0.28 eV, the rate of D uptake is defined by the kinetic reactions on the surface [58]. We have used a chemisorption energy of E_D = 0.8 eV and an energy barrier for a D atom to migrate from the surface into the bulk of E_A = 1.5 eV that were defined by the speed of uptake observed on the *'no-He'* side of '*6.8 % He + 1700 K + W dam'* sample and are close to the values used in [58]. These energies combined with the pre-factor of the diffusion coefficient equal to 1.34×10^{-7} m^2/s and the diffusion energy equal to 0.2 eV [54], define the set of non-defect related parameters used in our simulation and thus define the rate of uptake of D from the W surface to the bulk. They were kept the same in both the *'no-He'* and the *'He'*-side of the sample. Using surface kinetics to define the boundary conditions drastically increases the computational cost of the simulation. To avoid this issue, we have instead used an artificial D ion flux with 5 eV/D energy that penetrates directly into the bulk and allows us to use the Dirichlet boundary condition (solute D concentration at surface equal to 0). The magnitude of this artificial ion flux was adjusted such that the rate of uptake of D to the bulk was the same as the one found by using the kinetic surface boundary condition. Such a way of treating the experimental D atom exposure allows us to drastically decrease computational cost of the simulation, without truly influencing the outcome of the simulation in regards to D transport and retention. We want to stress here that this approach is only possible because we used the same temperature for all D loading experiments. For variable sample temperature the appropriate ion flux would need to be adjusted.

Before we start describing our simulation results for both samples, we must also define what were the defect depth distributions used in our simulation. The defects that are caused by W irradiation were modelled as having a step profile that extends down to 2 μm based on the Heaviside function with a transition size of around 0.15 μm instead of the calculated damage depth profile. This flat profile is justified due to the fact that the W irradiation fluence used to create the displacement damage was large enough for displacement damage saturation to occur [22]. A depth distribution equal to the He implantation profile calculated by SRIM [24] was taken as the defect

depth profile caused by the He implantation, seen in figure 4. Both of the described depth distributions were normalized to one at their respective maximum.

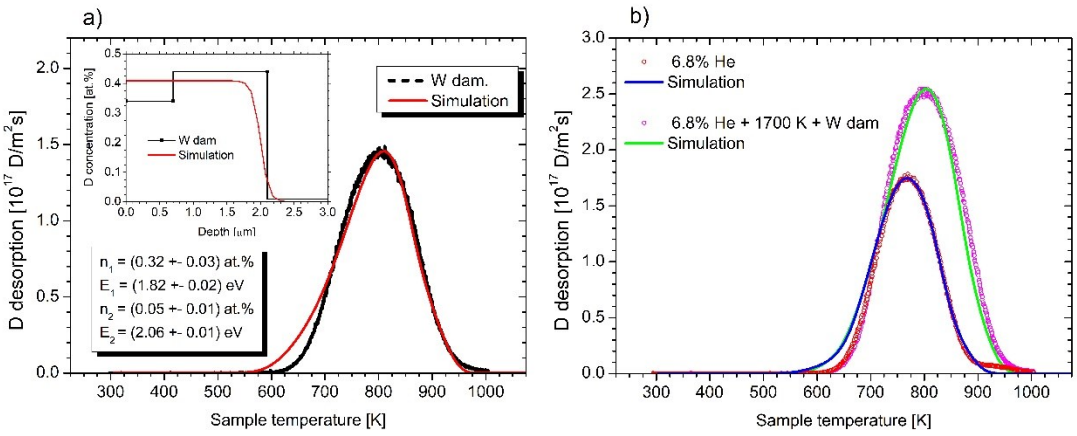

Figure 13: (a) Comparison of the measured and the simulated D thermal desorption spectra and the D depth profiles, as inserted graph, for the 'W dam', which is the 'no-He' side of the '6.8 % He + 1700K + W dam' sample. The insert gives the trap densities and the respective de-trapping energies for the two trap types used in the simulation. (b) Simulation and measured D thermal desorption spectra for the '6.8 % He + 1700 K + W dam' He' side of the sample and for the '6.8 % He' sample.

We first recreated the D depth profile and D desorption spectrum of the *'no-He'* side of the '*6.8 % He + 1700 K + W dam'* sample, referred as '*W dam'*, as the results provide information on the number of defect types created by the W irradiation, number of their fill-levels and their respective fill-level de-trapping energies. The best model fit of the experimental results can be seen in Fig. 13a. It was achieved when using two defect types, each with one fill-level with de-trapping energies equal to 1.82 and 2.06 eV, respectively. The defect concentrations used were equal to 0.32 at.% and 0.05 at.%. This set of parameters that describes the displacement damage created by W irradiation at room temperature and subsequent D atom loading at 600 K is consistent with previous simulation results [46, 58, 59].

To replicate the experimental results of the He-implanted side of the '*6.8 % He + 1700 K + W dam'* sample we used the same defect types that describe the W-irradiation-created defect as in the *'no-He'* side of the sample, but with the addition of a He-induced

defect with one fill-level with a de-trapping energy equal to 1.74 eV and a defect concentration of 1.6 at.%. The comparison of the experimental results and the simulation can be seen in figure 13b for the D desorption spectrum and in figure 14a-f for the D depth profiles. From the D desorption spectrum, we can see that the He-induced defect actively de-traps D during the TDS measurement at around 800 K, which means that the overall D desorption spectrum shape is largely un-affected by He. The effect of He is much clearer and interesting when we follow the D depth profiles measured at different exposure times i.e. D fluences. We observed that the D penetrates beyond the He implantation zone before it reaches its maximum concentration. D is hence taken up by the He-induced defect and the W-created defects in greater depth deeper at the same time. This can be explained with the simulation by the combination of a relatively low de-trapping energy of the He-induced defect and its comparably large concentration. We can also see that the distribution of the He-induced defect (equal to the He implantation profile) describes both the TDS and the D depth profile quite well (figure 13b and 14). Interestingly, slightly lower de-trapping energy and large defect density induced by the He does not show up in a peak shift of D thermal desorption spectrum.

We have also simulated the TDS spectra for the '*6.8 % He'* sample as irradiated. For that sample we have observed a shift in the position of the desorption peak by 30 K, as compared to the *'He + W dam'* samples. As the He will cause unavoidably displacement damage we have kept the same de-trapping energies responsible for D trapping in displacement damaged defects being 1.82 eV and 2.08 eV with maximum trap concentrations of 0.47 at.% and 0.05 at.%, respectively. We have assumed that the depth profiles of the trap concentrations are the same as the ones obtained by SRIM and are also shown in figure 4. Additionally to this we have added another trap with maximum trap concentration of 1.6 at.% and de-trapping energy of 1.67 eV. The depth profile of this trap was assumed to be the same as the SRIM calculated He depth profile, shown in figure 4. For these parameters we have obtained good agreement of the simulated D desorption spectra with the measured ones, as can be seen in figure 13. We have obtained also good agreement of the simulation with the D depth profiles as a function of D fluence, which we do not show since the spectra look very similar to the ones shown in figure 14, down to the depth of 1 μm.

In summary, modelling of the experimental depth profiles and thermal desorption spectra for the as He implanted as well as for the 1700 K annealed '*He + W dam'* sample indicated that

He implantation adds one more defect type that shows a slightly smaller de-trapping energy for D but has (for our He concentrations) a comparably large defect density.

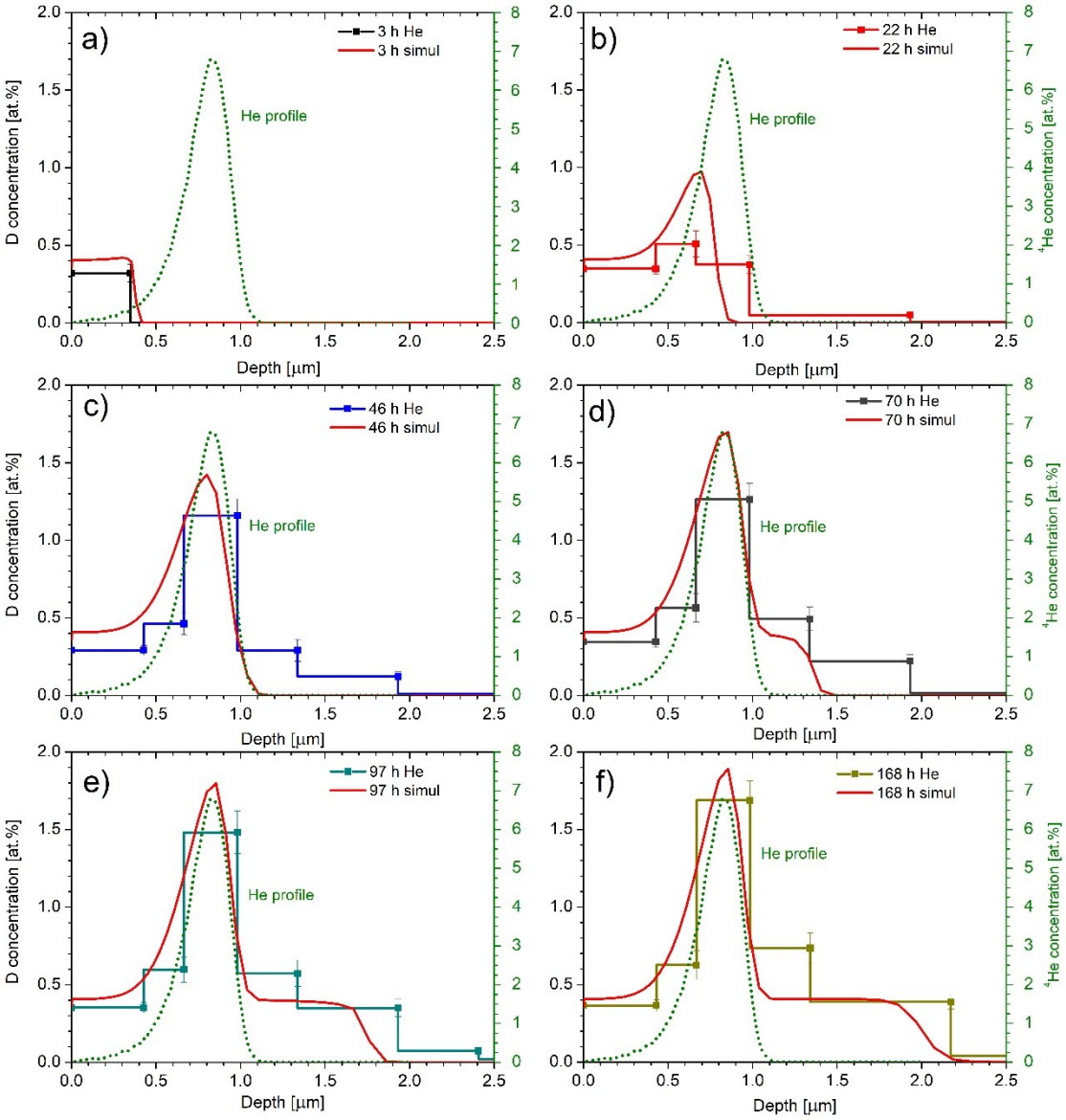

Figure 14: Comparison of the measured and the simulated D depth profiles for the 'He' side on the '6.8 % He + 1700 K + W dam' sample at different exposure times to the D atom beam at 600 K.

6. Discussion

6.1 He as implanted and 800 K annealed

The first important finding of the present study with W pre-irradiated (self-damaged) W irradiated at 300 K with different He fluences (2×10^{20} He/m^2, 7×10^{20} He/m^2 and 14×10^{20} He/m^2) is an increase of D concentration with the calculated He concentration. For atom loading at 600 K the maximum D concentrations of 0.49, 0.84 and 1.1 at.% were measured for calculated He concentrations of 1 at.%, 3.4 at.% and 6.8 at.%, respectively (figure 7a). The obtained D concentrations were all higher as compared to the maximum achievable D concentration of about 0.37 at.% for highly self-damaged W for the same exposure conditions. The D retention attributed to He increases almost linearly with the He fluence with a ratio of 0.29 retained D atoms per retained He atom for our exposure conditions. From the TDS spectra we can also conclude that the de-trapping energy of D from the He + W irradiated samples is not much different compared to only W irradiated, since the peak position and shape stayed the same (figure 10), only D retention increased. We observed similar D retention and D concentration increase also for only He implanted sample, as irradiated (figure 4). Only the D desorption spectrum shows a small shift of 30 K in the D desorption peak position to lower temperatures for the '*6.8 % He'* sample as irradiated as compared to '*6.8 % He + W dam'* sample. This is an indication that the de-trapping energy changed which is a hint for a new type of defect when going from He as irradiated to He + W irradiated and annealed at 800 K. From the STEM images we observed that we have in the He area a dense dislocation network. However, vacancies and vacancy clusters or mixed HeV clusters cannot be visualized by this technique. Therefore, the question is, what kind of defects we have created in the He implantation zone, where we observe a substantially larger D atom trapping as compared to highly self-damaged W.

According to theory He feels strong attraction to defects [8, 9]. Therefore, we can assume that the implanted He formed individual He-vacancies or He-vacancy clusters with defects created during He irradiation and with pre-existing defects. Debelle et al. [60] studied by positron annihilation spectroscopy (PAS) the created defects in W irradiated at room temperature by 800 keV He ions with fluences up to 5×10^{20} He/m^2, i.e. very similar conditions as compared to the present work. They focused on the first 700 nm from the surface which they called the track region where the ratio of He concentration and displacement damage is low. This zone is before the Bragg peak, where the damage reaches its maximum but also most of the He ions are stopped and hence

the ratio of He concentration and displacement damage is larger. They observed creation of single vacancy-type defects in the as irradiated samples. When these He containing samples were annealed, PAS showed a change in the nature of defects above 523 K transforming from single vacancy-like defects into larger vacancy-type defects. The effect was clearly pronounced for fluences of 1×10^{20} He/m^2 and 5×10^{20} He/m^2. The concentration of vacancy cluster-like defects increased with the He fluence, changing also the defect depth profile. The nature of defects and their evolution was also modelled by Object Kinetic Monte Carlo [49, 61] for those exposure conditions. According to the modelling [49] the track region contains 25.4 % of point defects and only 3.75 % of He atoms, the rest of the defects and He is around the Bragg peak. The simulation showed that even though there is only 3.75 % of He in the track region the presence of He substantially influenced the formation of defects and number of vacancies and vacancy clusters. The modelling showed that He is playing an important role on recombination, by forming mixed He-self-interstitial clusters and a larger number of vacancies is left during the He implantation which would recombine in the case without He. Therefore, we can say that He is stabilizing the defects. During the annealing up to 900 K the He-self-interstitial clusters recombine with vacancies and at the same time the number of He-vacancy and He-vacancy clusters increases because He is released from self-interstitial clusters. The microstructure is left with a large number of vacancy clusters (V_m) and mixed He-vacancy (He_nV_m) clusters with dominantly very small and single vacancy-He (He_nV) clusters. In the case without He, only larger vacancy clusters (V_m) are obtained. At 10^{20} ion fluence the cluster size distribution peaks at 300 vacancies in a cluster. The simulation also shows that the larger the He fluence the larger concentration of He_nV and He_nV_m is found.

Based on these simulation results we can assume that also for our conditions we have a large number of He-vacancy clusters, and that their concentration increases with the He fluence. The shift in the D desorption peak position by 30 K between the '*6.8 % He'* sample as irradiated and '*6.8 % He + W dam'* could be explained by the change of the defects due to the annealing for the second case. The shift in the desorption temperature is rather small which is in agreement with the DFT calculations for He_xVH_y complexes [9] showing that the D binding energy does neither change much compared to a single vacancy nor with the increase of He atoms in the cluster. From the simulation we can assume that this shift corresponds to a difference in de-trapping energy of 0.05 eV. The attraction of H to the HeV complex is larger compared to a He-free vacancy which

at the same time allows also for more trap sites around He_xV_y complex [15]. More trap sites around He complexes is presumably also the reason for larger D retention increasing with He fluence in 'He' side of the *He + W dam'* sample as compared to only '*no-He'* side.

6.2 1700 K annealed samples

In order to isolate the effect the presence of He has from the effect the creation of displacement damage we have annealed two *'3.4 at.% He + W dam'* and two 6.8 at.% He containing samples to 1700 K for 30 min. At such high temperatures it was shown that displacement damage is annealed out [48] whereas He stays in the bulk of W [25, 30]. Chernikov et al. [50] showed that at such annealing temperatures (above 1523 K) visible He bubbles are created in a W sample He irradiated to 600 appm. Creation of He bubbles was already suggested by Debelle et al. [30] where a 500 keV ^{3}He irradiated W sample showed peaking of the He depth profile with 50 % increase in local He concentration after annealing to 1773 K. From Harrison et al. [62] one can also learn that for samples irradiated by He at 773 K, the He concentration and created dpa does not influence much on the bubble size. However, the annealing or irradiation temperature does influence bubble size substantially.

If we now correlate the observations from literature with our present study we indeed observed negligible D retention outside the SRIM calculated He peak (figure 8), which confirms the reduction of displacement damage by 1700 K annealing by 80 %. Annealing of defects was also confirmed by STEM analysis on the '*3.4 % He + W dam'* sample where almost no dislocation lines and loops were left outside the He zone. At the same time TEM micrographs showed that after annealing He bubbles were created in the He irradiation zone. The bubble size measured by TEM was approximately 1.5 nm in diameter which agrees well with the study of Chernikov et al. for this annealing temperature [50]. From [62, 50] we can also assume that the bubble size is similar for the 3.4 at.% and for the 6.8 at.%. Contrary to the annealing of the displacement damage in front and beyond the He zone we have still observed substantial D retention where the He bubbles were observed by TEM. We also observe a change in the D concentration depth profile after annealing. Before annealing a broad D concentration peak in the D depth profile was measured and after annealing at 1700 K the peak was significantly narrower (figure 8). D concentration increased from 1.1 at.% to 1.35 at.% obtaining a 20% increase in local D concentration. Because Debelle et al. [30] observed an increase in the ^{3}He concentration and a

narrowing of the profile after annealing we attribute the observed increase in local D concentration to agglomeration of He and creation of He bubbles during annealing. With the fact that the TDS peak shape did not change (figure 10) for the '*6.8 % He + 1700 K + W dam'* sample as compared to *'6.8 % He + W dam'* and 800 K annealed, we can say that the He-vacancy cluster exhibit similar H binding energy as compared to He bubbles. This is another clear indication that D correlates strongly with the He zone, namely D resides where the He is present. This supports also the results from MD simulations where it was shown that hydrogen is attracted to the periphery of a He bubble where it is also strongly bound [17]. From this we can conclude that He does influence D retention either by creating different vacancy clusters with He during the implantation or the He itself influences D retention. Which of these two effects is the dominant we cannot say from our study and is a motivation for further studies.

6.3 D transport in He containing W sample

When comparing the D transport on the *'He'* and the *'no-He'* side of the sample no substantial difference in the diffusion speed was observed for both the 'He + W dam' samples (figures 5a and 6) where we assume we had mainly smaller He-vacancy clusters and the '*6.8 % He + 1700 K + W dam'* sample (figure 9) where He bubbles were observed. From this we conclude that neither He-vacancy clusters nor He bubbles act as diffusion barrier despite the fact that additional trapping sites are available. This at first glance surprising observation can be understood by a closer look at the D uptake on the annealed sample: At the same time as the D diffusion front continued beyond the He zone into the W damage zone, the D concentration still increased in the He zone. This was to the author's knowledge never experimentally observed before and means that He differently influences on HI trapping as compared to the only W irradiated and hence displacement damaged W. In the latter case it is typically observed that a diffusion front with constant D concentration is moving deeper into the sample. The simulation of the data from figure 9 showed us that we were able to get a good agreement with the experimental D depth profiles and D desorption spectrum only when the de-trapping energy in the He zone was set slightly lower (1.74 eV) as compared to the de-trapping energy for the traps due to W ion irradiation (1.82 and 2.06 eV, figure 14) which we assume are vacancy clusters and voids [63]. Therefore, the He zone acted similarly as a non-saturable trap that was filling even after the diffusion front went further into depth. From the MD simulations for hydrogen trapping around a He bubble, a binding energy for D between 1.5 eV and 2.5 eV [17] was calculated. Assuming an

energy for diffusion E_{diff} of 0.28 eV as recently determined experimentally [64] we get a binding energy of 1.46 eV from the de-trapping energy of 1.74 eV from our simulation. Assuming E_{diff} = 0.20 eV as derived by DFT [54] a binding energy of 1.54 eV is obtained. In both cases the binding energy obtained here is on the lower side of the binding energies as determined by MD simulation. This low binding energy also indicates that by using a lower exposure temperature we could possibly get an even higher D concentrations since thermal de-trapping apparently plays an important role for the He induced trap for our exposure conditions. Moreover, the fact that D concentration was increasing also during further D transport into depth made us think about the D exposures of the '*He + W dam'* samples (figure 5). Despite the fact that all the D concentrations are higher as compared to highly self-damaged W, this behavior of this sample indicates that we might not be in saturation for '*He + W dam'* samples and D concentration would continue to increase with additional D atom exposure. However, since we obtain in the '6.8 % *He + W dam'* and '6.8 % *He + W dam + 1700 K'* similar D amount due to He presence we believe we are in saturation in all cases.

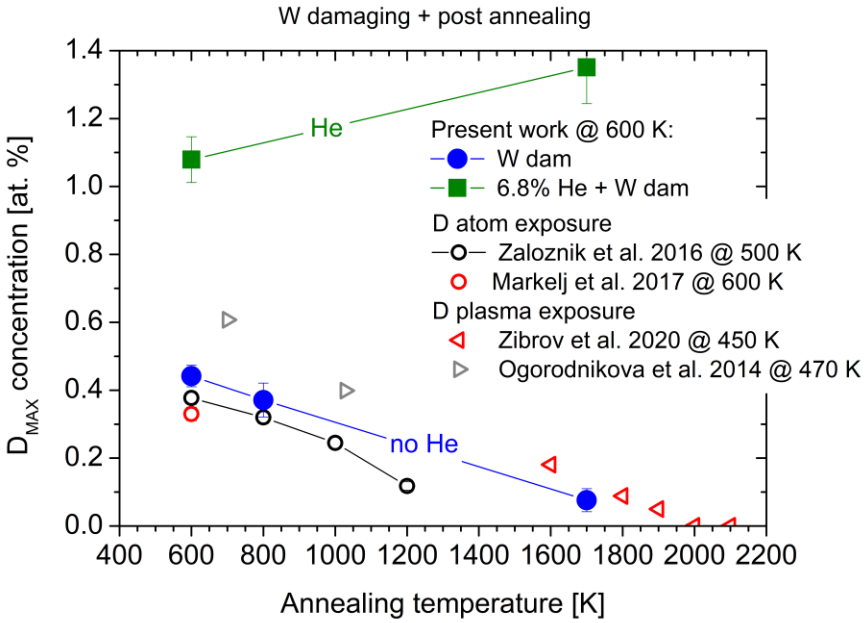

Figure 15: Maximum D concentrations obtained from final D depth profiles shown in figures 4 and 8 on the 'He' sides of the '6.8 % He' and '6.8 % He + W dam + 1700 K' samples, respectively. The same is shown for the 'no-He' sides for the '6.8 % He + 1700 K + W dam', '6.8 % He + W dam' and '6.8 % He + W dam + 1700 K ' samples, respectively, where the first

data point is shown at 600 K, which is the exposure temperature, the second is at 800 K due to stepped annealing procedure and the last one is due to annealing at 1700 K. For comparison we also show literature post-damaging annealing data from Založnik et al. [44] *and Markelj et al.* [42]*, where in both cases D atom exposure was performed and Zibrov et al.* [51] *and Ogorodnikova et al.* [65]*, where plasma exposure was performed, at the indicated exposure temperatures.*

6.4 Influence of He on D retention in fusion devices

What do the present results tell us about the influence of He on steady state fuel retention in the bulk of tungsten as a plasma facing material in a future fusion reactor such as DEMO? This is the first experimental study where absolute amounts of D retention with respect to implanted He amount and He concentrations were determined. At this point we need to stress that these values are not valid near the surface where material erosion, re-deposition, co-deposition of HI and He, implantation of seeding impurities and an evolving surface morphology will play the major role. The aim of this study was to derive the influence of He in the bulk of tungsten, hundreds of micrometers below the surface. We expect that the He interaction is the same for all HIs due to the similar electronic structure, considering that the observed phenomena and theoretical calculations are not isotope dependent. Therefore, we can state that for He concentrations below 10000 appm the influence of He on T retention is negligible in displacement-damaged W at DEMO relevant exposure temperatures of 600 K. At larger He concentrations we found a clear measurable effect. According to the presently available calculations He concentrations of 600 – 700 appm are predicted to be produced in W after 5 years of operation due to nuclear reactions with neutrons [5] and T decay [4]. From this we conclude that in areas in DEMO where temperatures will be below 900 K [66], like in the first wall, the influence of He on D transport and retention will be marginal and will be dominated by the displacement damage the neutrons will cause. However, in the high heat loads and particle flux areas like the divertor with temperature excursions above 1200 K, the displacement damage will be annealed but the influence of He on T retention will remain. The difference in displacement damage and He annealing and their effect on the evolution of maximum D concentration with the annealing temperature is shown in figure 15. We compare there the final D concentrations obtained on the *'He'* and *'no-He'* sides of the different variations of the 6.8 % He samples. We compare also the present results on the *'no-He'* side of the '*6.8 % He + W dam'* sample to other displacement damage annealing studies performed by exposure to D atoms [44,

42] and D plasma [65, 51]. We see that for D atom exposures we get good agreement to previous studies, with decrease of D concentration with annealing temperature. The obtained D concentrations for the plasma exposures are higher as compared to the D atom exposures. This is attributed to the lower exposure temperature (450-470 K) and higher D ion flux for the plasma experiments, where traps with lower de-trapping energy can be populated [63], which is not the case for D atom exposure at 600 K. Still we observe similar, almost linear decrease of D concentration at high annealing temperature of 1700 K, as was observed in a recent study by Zibrov et al. [51]. For the *'He'* side no decrease in D concentration is observed after annealing to 1700 K. We observe even an increase by 20 %, which is due to accumulation of He at high temperatures. This difference in the behaviour of He and irradiation damage with respect to D retention is important since the present study clearly shows that He is not annealed out as is the case for the irradiation damage [48]. He will stay in the material and will not be desorbed even when the material reaches 1700 K. It will accumulate with time and at high temperatures it will form bubbles [62].

We want to stress here that despite the fact that neither the fluxes nor the energies of our D atom beam resemble fluxes or energies expected for the DEMO first wall the above statement holds true. For expected particle fluxes in the range of 10^{18} to 10^{20} D/m^{2}s [67, 68] and wall temperatures up to 600 K retention is determined by the trap density and not the solute HI concentration [69]. Hence, our gentle atom loading procedure can directly be used to predict retention for the given temperature. This does not hold true for higher temperatures that will prevail in the high heat flux areas of the divertor. At these temperatures retention is dominated by the balance between the HI influx and thermal de-trapping [69]. The retention values from figure 15 might therefore only be considered as lower limits. Several orders of magnitude higher HI fluxes can rise retention substantially [69]. However, material erosion, re-deposition, co-deposition of HI and He, implantation of seeding impurities together with an evolving surface morphology makes a prediction of the net HI influx into the bulk impossible. The here given ratio of 0.29 D/He can therefore not be applied. However, the qualitative observation that displacement damage will anneal out while He will accumulate remains valid.

7. Conclusions

The influence of different He concentrations, ranging from 1 at.% to 6.8 at.%, on D retention and transport was studied. He was implanted with 500 keV up to a depth of 0.84 μm, which created displacement damage at the damage peak between 0.17 and 1.2 dpa, respectively. In some of the samples, displacement damage was additionally created by 20 MeV W ion irradiation. The study was performed by measuring D depth profiles *in situ* during D atom exposure at 600 K utilizing NRA. We observe increased D concentration in the He zone being three times higher than the D concentration obtained in the *'no-He'* and only displacement-damaged samples for the highest implanted ^{4}He concentration of 6.8 at.%. In the presence of displacement damage, we expect that He is trapped in the form of He-vacancy clusters. For the first time we determine absolute quantitative numbers, which one can use to predict the influence of He on T retention in the bulk of tungsten of future tungsten-based plasma facing components. We obtained a D over He ratio of 0.29 for our exposure conditions. Comparing the D depth profiles on the *'He'* and *'no-He'*-implanted samples allowed us to study D transport and the possible effect of He on it. We concluded that He does not act as a diffusion barrier for D atom transport. In order to study how macroscopic He bubbles influence D transport in tungsten as compared to as implanted He, samples with 6.8 at.% and 3.4 at.% He concentration were annealed for 30 min at 1700 K to create macroscopic bubbles of 1.5 nm in diameter. Although the displacement damage annealed out, D concentration observed in the He-bubble-containing zone was even slightly larger than in the non-annealed sample. With this we obtained almost four times larger D concentrations as compared to highly self-damaged W loaded with D atoms at the same loading conditions. TDS preformed on these samples showed that the D desorption peak keeps the same shape as compared to the only W irradiated sample. From this we concluded, in combination with rate equation modelling, that the de-trapping energy for D from He-vacancy clusters and or He bubbles is similar or even slightly lower than the de-trapping energy for displacement damaged tungsten. We have concluded that a ratio of 0.29 D/He is a good proxy for the first wall where temperatures are expected to be low (< 900 K) and D retention does not depend on flux. Under these conditions HI retention will be dominated by displacement damage. In the divertor the He effect will be larger than in the main wall because He does not lose its capacity to trap hydrogen after annealing at high elevated temperature while displacement damage will anneal out. A more quantitative statement remains motivation for further studies.

Acknowledgment

We would like to thank M. Kelemen and dr. P. Vavpetič at Jožef Stefan Institute and T. Dürbeck, J. Dorner and M. Fußeder at Max-Planck-Institut für Plasmaphysik for their technical support.

This work has been carried out within the framework of the EUROfusion Consortium and has received funding from the Euratom research and training programme 2014-2018 and 2019-2020 under grant agreement No 633053. The views and opinions expressed herein do not necessarily reflect those of the European Commission. The authors acknowledge the support from the Slovenian Research Agency (research core funding No. P2-0405).

Bibliography

[1] K. Hammond, "Helium, hydrogen, and fuzz in plasma-facing materials," *Materials Research Express,* vol. 4, p. 104002, 2017.

[2] M. Baldwin, R. Doerner, W. Wampler, D. Nishijima, T. Lynch and M. Miyamoto, "Effect of He on D retention in W exposed to low-energy, high-fluence (D, He, Ar) mixture plasmas," *Nucl. Fusion ,* vol. 51, p. 103021, 2011.

[3] M. Miyamoto, S. Mikami, H. Nagashima, N. Iijima, D. Nishijima, R. Doerner, N. Yoshida, H. Watanabe, Y. Ueda and A. Sagara, "Systematic investigation of the formation behavior of helium bubbles in tungsten," *Journal of Nuclear Materials,* vol. 463, p. 3, 2015.

[4] M. Shimada and B. Merrill, "Tritium decay helium-3 effects in tungsten," *Nuclear Materials and Energy,* vol. 12, pp. 699-702, 2017.

[5] M. Gilbert and J.-C. Sublet, "Neutron-induced transmutation effects in W and W-alloys in a fusion environment," *Nuclear Fusion,* vol. 51, p. 043005, 2011.

[6] H. Ullmaier, "The influence of helium on the bulk properties of fusion reactor structural materials," *Nucl. Fusion,* vol. 24, p. 1039, 1984.

[7] C. Becquart and C. Domain, "Migration Energy of He in W Revisited by Ab Initio Calculations," *Physical Review Letters,* vol. 97, p. 196402, 2006.

[8] H.-B. Zhou, Y.-H. Li and G.-H. Lu, "Modeling and simulation of helium behavior in tungsten: A first-principles investigation," *Computational Materials Science,* vol. 112, p. 487–491, 2016.

[9] C. Becquart and C. Domain, "A density functional theory assessment of the clustering behaviour of He and H in tungsten," *Journal of Nuclear Materials ,* vol. 386–388, p. 109–111, 2009.

[10] F. Sefta, K. Hammond, N. Juslin and B. Wirth, “Tungsten surface evolution by helium bubble nucleation, growth and rupture,” *Nucl. Fusion,* vol. 53, p. 073015, 2013.

[11] S. Gilliam, S. Gidcumb, N. Parikh, D. Forsythe, B. Patnaik, J. Hunn, L. Snead and G. Lamaze, “Retention and surface blistering of helium irradiated tungsten as a first wall material,” *Journal of Nuclear Materials,* vol. 347, p. 289–297, 2005.

[12] Y. Ueda, M. Fukumoto, J. Yoshida, Y. Ohtsuka, R. Akiyoshi, H. Iwakiri and N. Yoshida, “Simultaneous irradiation effects of hydrogen and helium ions on tungsten,” *Journal of Nuclear Materials,* vol. 386–388, p. 725–728, 2009.

[13] V. Alimov, W. Shu, J. Roth, K. Sugiyama, S. Lindig, M. Balden, K. Isobe and T. Yamanishi, “Surface morphology and deuterium retention in tungsten exposed to low-energy, high flux pure and helium-seeded deuterium plasmas,” *Physica Scripta,* vol. T138, p. 014048, 2009.

[14] H. Lee, A. Haasz, J. Davis and R. Macaulay-Newcombe, “Hydrogen and helium trapping in tungsten under single and sequential irradiations,” *Journal of Nuclear Materials,* vol. 360, p. 196–207, 2007.

[15] H.-B. Zhou, Y.-L. Liu, S. Jin, Y. Zhang, G.-N. Luo and G.-H. Lu, “Towards suppressing H blistering by investigating the physical origin of the H–He interaction in W,” *Nuclear Fusion ,* vol. 50, p. 115010, 2010.

[16] N. Juslin and B. Wirth, “Molecular dynamics simulation of the effect of sub-surface helium bubbles on hydrogen retention in tungsten,” *Journal of Nuclear Materials,* vol. 438, p. S1221–S1223, 2013.

[17] Z. Bergstrom, M. Cusentino and B. Wirth, “A Molecular Dynamics Study of Subsurface Hydrogen-Helium Bubbles in Tungsten,” *Fusion Science and Technology,* vol. 71, pp. 122-135, 2017.

[18] M. Ialovega, E. Bernard, R. Bisson, C. Martin, R. Sakamoto, A. Kreter, E. Hodille, T. Angot and C. Grisolia, “Hydrogen trapping in tungsten: impact of helium irradiation and thermal cycling,” *Phys. Scr.,* vol. T171, p. 014066, 2020.

[19] H. Iwakiri, K. Morishita and N. Yoshida, “Effects of helium bombardment on the deuterium behavior in tungsten,” *Journal of Nuclear Materials ,* vol. 307–311, p. 135–138, 2002.

[20] I. Arkhipov, S. Kanashenko, V. Sharapov, R. Zalavutdinov and A. Gorodetsky, “Deuterium trapping in ion-damaged tungsten single crystal,” *Journal of Nuclear Materials,* vol. 363–365, p. 1168–1172, 2007.

[21] S. Markelj, T. Schwarz-Selinger and A. Založnik, “ Hydrogen isotope accumulation in the helium implantation zone in tungsten,” *Nuclear Fusion,* vol. 57, no. 2017., p. 064002, 2017.

[22] O. V. Ogorodnikova and V. Gann, “Simulation of neutron-induced damage in tungsten by irradiation with energetic self-ions,” *J. Nucl. Mater.,* vol. 460, p. 60, 2015.

[23] V. Alimov, Y. Hatano, B. Tyburska-Püschel, K. Sugiyama, I. Takagi, Y. Furuta, J. Dorner, M. Fußeder, K. Isobe, T. Yamanishi and M. Matsuyama, “Deuterium

retention in tungsten damaged with W ions to various damage levels," *J. Nucl. Mater.,* vol. 441, p. 280–285, 2013.

[24] J. Ziegler, "www.srim.org.," [Online].

[25] E. Markina, M. Mayer, S. Lindig and T. Schwarz-Selinger, "Influence of MeV helium implantation on deuterium retention in self-ion implanted tungsten," *Physica Scripta ,* vol. T159, p. 014045, 2014.

[26] A. Manhard, M. Balden and S. Elgeti, "Quantitative Microstructure and Defect Density Analysis of Polycrystalline Tungsten Reference Samples after Different Heat Treatments," *Pract. Metallorg. ,* vol. 52, p. 437, 2015.

[27] A. Manhard, G. Matern and M. Balden, "A Step-By-Step Analysis of the Polishing Process for Tungsten Specimens," *Pract. Metallorg. ,* vol. 50, pp. 5-16, 2013.

[28] T. Schwarz-Selinger, "Deuterium Retention in MeV Self-Implanted Tungsten: Influence of Damaging Dose Rate," *Nuclear Energy and Materials,* vol. 12, p. 683–688 , 2017.

[29] ASTM Int'l E521-16, "Standard practice for neutron radiation damage simulation by charge-particle irradiation," in *Annual Book of ASTM Standards vol 12.02*, Philadelphia, PA, American Society for Testing and Materials, 2016, p. p 8.

[30] A. Debelle, M. Barthe, T. Sauvage, R. Belamhawal, A. Chelgoum, P. Desgardin and H. Labrim, "Helium behaviour and vacancy defect distribution in helium implanted tungsten," *Journal of Nuclear Materials,* vol. 362, p. 181–188, 2007.

[31] S. Markelj, A. Založnik, T. Schwarz-Selinger, O. V. Ogorodnikova, P. Vavpetič, P. Pelicon and I. Čadež, "In situ NRA study of hydrogen isotope exchange in self-ion damaged tungsten exposed to neutral atoms," *J. Nucl. Mater.,* vol. 469, p. 133–144, 2016.

[32] M. Schlüter, C. Hopf, T. Schwarz-Selinger and W. Jacob, "Temperature dependence of the chemical sputtering of amorphous hydrogenated carbon films by hydrogen," *Journal of Nuclear Materials,* vol. 376, p. 33–37, 2008.

[33] T. Schwarz-Selinger, A. Von Keudell and W. Jacob, "Novel method for absolute quantification of the flux and angular distribution of a radical source for atomic hydrogen," *Journal of Vacuum Science & Technology A: Vacuum, Surfaces, and Films,* vol. 18, p. 995–1001, 2000.

[34] B. Wielunska, M. Mayer, T. Schwarz-Selinger, U. von Toussaint and J. Bauer, "Cross Section Data for the D(3He,p)4He Nuclear Reaction from 0.25 to 6MeV," *Nuclear Instruments and Methods in Physics Research Section B: Beam Interactions with Materials and Atoms,* vol. 371, pp. 41-45, 2016.

[35] M. Mayer, E. Gauthier, S. K and U. v. Toussaint, *Nucl. Instr. and Meth. in Phys. Res. B,* vol. 267, p. 506, 2009.

[36] M. Mayer, "RESOLNRA: A new program for optimizing the achievable depth resolution of ion beam analysis methods," *Nuclear Instruments and Methods in Physics Research Section B: Beam Interactions with Materials and Atoms,* vol. 266, p. 1852–1857, 2008.

[37] B. Wielunska, M. Mayer and T. Schwarz-Selinger, "Optimization of the depth resolution for deuterium depth profiling up to large depths," *Nuclear Instruments*

and Methods in Physics Research Section B: Beam Interactions with Materials and Atoms, vol. 387, p. 103, 2016.

[38] M. Meyer, "SIMNRA User's Guide, Report IPP 9/113," Max-Planck-Instutut für Plasmaphysik, Garching, Germany, Available: http://www.rzg.mpg.de/~mam/., 1997.

[39] K. Schmid and U. von Toussaint, *Nucl. Instr. and Meth. in Phys. Res. B,* vol. 281, p. 64, 2012.

[40] E. Salançon, T. Dürbeck, Schwarz-Selinger, F. Genoese and W. Jacob, *J. Nucl. Mater.,* vol. 376, p. 160, 2008.

[41] A. Šestan, P. Jenuš, S. Krmpotič, J. Zavašnik, J. Zavašnik and M. Čeh, "The role of tungsten phases formation during tungsten metal powder consolidation by FAST: Implications for high-temperature application," *Mater. Charact.,* vol. 138, p. 308–314, 2018.

[42] S. Markelj, T. Schwarz_Selinger, A. Zaloznik, M. Kelemen, P. Vavpetic, P. Pelicon, E. Hodille and C. Grisolia, "Deuterium retention in tungsten simultaneously damaged by high energy W ions and loaded by D atoms," *Nucl. Mater. Energ.,* vol. 12, pp. 169-174, 2017.

[43] S. Markelj, O. V. Ogorodnikova, P. Pelicon, T. Schwarz-Selinger and I. Cadez, "Temperature dependence of D atom adsorption on polycrystalline tungsten," *Appl. Surf. Sci. ,* vol. 282, pp. 478-486, 2013.

[44] A. Založnik, S. Markelj, T. Schwarz-Selinger, Ł. Ciupiński, J. Grzonka, V. P. and P. Pelicon, "The influence of the annealing temperature on deuterium retention in self-damaged tungsten," *Phys. Scr.,* vol. T167, p. 014031, 2016.

[45] T. Schwarz-Selinger, J. Bauer, S. Elgeti and S. Markelj, "Influence of the presence of deuterium on displacement damage in tungsten," *Nuclear Materials and Energy,* vol. 17, p. 228–234, 2018.

[46] M. Pečovnik, S. Markelj, A. Založnik and T. Schwarz-Selinger, "Influence of grain size on deuterium transport and retention in self-damaged tungsten," *J. Nucl. Mater.,* vol. 513, p. 198, 2019.

[47] M. Pecovnik, S. Markelj, M. Kelemen and T. Schwarz-Selinger, "Effect of D on the evolution of radiation damage in W during high temperature annealing," *Nuclear Fusion,* vol. 60, p. 106028, 2020.

[48] F. Ferroni, X. Yi, K. Arakawa, S. Fitzgerald, P. Edmondson and S. Roberts, "High temperature annealing of ion irradiated tungsten," *Acta Materialia,* vol. 90, p. 380–393, 2015.

[49] A. De Backer, P. Lhuillier, C. Becquart and M. Barthe, "Modelling of the implantation and the annealing stages of 800keV 3He implanted tungsten: Formation of nanovoids in the near surface region," *Journal of Nuclear Materials ,* vol. 429, p. 78–91, 2012.

[50] V. Chernikov, J. Lakhotkin, H. Ullmaie, H. Trinkaus, P. Jung and H. Bierfeld, "Helium-induced swelling in tungsten during postimplanatation annealing," *J. Nucl. Mater.,* Vols. 212-215, p. 375, 1994.

[51] M. Zibrov, T. Dürbeck, W. Egger and M. Mayer, “High temperature recovery of radiation defects in tungsten and its effect on deuterium retention,” *Nuclear Materials and Energy,* vol. 23, p. 100747, 2020.

[52] S. Das, H. Yu, E. Tarleton and F. Hofmann, “The effect of helium implantation on the deformation behaviour of tungsten: X-ray micro-diffraction and nanoindentation,” *Scientific Reports,* vol. 9, p. 18354, 2019.

[53] E. A. Hodille, Y. Ferro, N. Fernandez, C. S. Becquart, T. Angot, J. M. Layet, R. Bisson and C. Grisolia, “Study of hydrogen isotopes behavior in tungsten by a multi trapping macroscopic rate equation model,” *Physica Scripta,* vol. T167, p. 014011, 2016.

[54] N. Fernandez, Y. Ferro and D. Kato, “Hydrogen diffusion and vacancies formation in tungsten: Density Functional Theory calculations and statistical models,” *Acta Materialia,* vol. 94, pp. 307-318, 2015.

[55] D. F. Johnson and E. A. Carter, “Hydrogen in tungsten: Absorption, diffusion, vacancy trapping, and decohesion,” *Journal of Materials Research,* vol. 25, pp. 315-327, 2010.

[56] K. Heinola, T. Ahlgren, K. Nordlund and J. Keinonen, “Hydrogen interaction with point defects in tungsten,” *Physical Review B,* vol. 82, p. 094102, 2010.

[57] J. Hou, X.-S. Kong, X. Wu, J. Song and C. S. Liu, “Predictive model of hydrogen trapping and bubbling in nanovoids in bcc metals,” *Nature Materials,* vol. 18, pp. 833-839, 2019.

[58] E. A. Hodille, A. Založnik, S. Markelj, T. Schwarz-Selinger, C. S. Becquart, R. Bisson and C. Grisolia, “Simulations of atomic deuterium exposure in self-damaged tungsten,” *Nucl. Fusion,* vol. 57, p. 056002, 2017.

[59] A. Založnik, S. Markelj, T. Schwarz-Selinger and K. Schmid, “Deuterium atom loading of self-damaged tungsten at different sample tempeatures,” *Journal of Nuclear Materials,* vol. 496, pp. 1-8, 2017.

[60] A. Debelle, M. Barthe and T. Sauvage, “First temperature stage evolution of irradiation-induced defects in tungsten studied by positron annihilation spectroscopy,” *Journal of Nuclear Materials,* vol. 376, p. 216–221, 2008.

[61] A. De Backer, C. Ortiz, C. Domain, M. Barthe and C. Becquart, “Spatial effects in the 800keV 3He implantation in W followed by isochronal annealing at 900K,” *Nuclear Instruments and Methods in Physics Research Section B,* vol. 303, pp. 87-90, 2013.

[62] R. Harrison, G. Greaves, J. Hinks and S. Donnelly, “A study of the effect of helium concentration and displacement damage on the microstructure of helium ion irradiated tungsten,” *Journal of Nuclear Materials,* vol. 495, p. 492–503, 2017.

[63] M. Pečovnik, E. Hodille, T. Schwarz-Selinger, C. Grisolia and S. Markelj, “New rate equation model to describe the stabilization of displacement damage by hydrogen atoms during ion irradiation in tungsten,” *Nucl. Fusion,* vol. 60, p. 036024, 2020.

[64] G. Holzner, T. Schwarz-Selinger, T. Dürbeck and U. v. Toussaint, “Solute diffusion of hydrogen isotopes in tungsten—a gas loading experiment,” *Phys. Scr.,* vol. T171, p. 014034, 2020.

[65] O. V. Ogorodnikova, Y. Gasparyan, V. Efimov, Ł. Ciupiński and J. Grzonka, "Annealing of radiation-induced damage in tungsten under and after irradiation with 20 MeV self-ions," *J. Nucl. Mater.,* vol. 451, no. 1-3, pp. 379-386, 2014.

[66] M. Rieth and e. al., "Recent progress in research on tungsten materials for nuclear fusion applications in Europe," *J. Nucl. Mater.,* vol. 432, p. 482–500, 2013.

[67] R. Behrisch, G. Federici, A. Kukushkin and D. Reiter, "Material erosion at the vessel walls of future fusion devices," *Journal of Nuclear Materials ,* vol. 313–316, p. 388–392, 2003.

[68] M. Tokar, "An assessment for the erosion rate of DEMO first wall," *Nucl. Fusion ,* vol. 58, p. 016016, 2017.

[69] E. Hodille, S. Markelj, M. Pecovnik, M. Ajmalghanc, Z. A. Piazza, Y. Ferro, T. Schwarz-Selinger and C. Grisolia, "Kinetic model for hydrogen absorption in tungsten with coverage dependent surface mechanisms," *Nuclear fusion ,* vol. 60, p. 106011, 2020.